339
5-11-66

IDO-17147

MASTER

NUCLEAR TECHNOLOGY BRANCHES QUARTERLY REPORT

July 1 - September 30, 1965

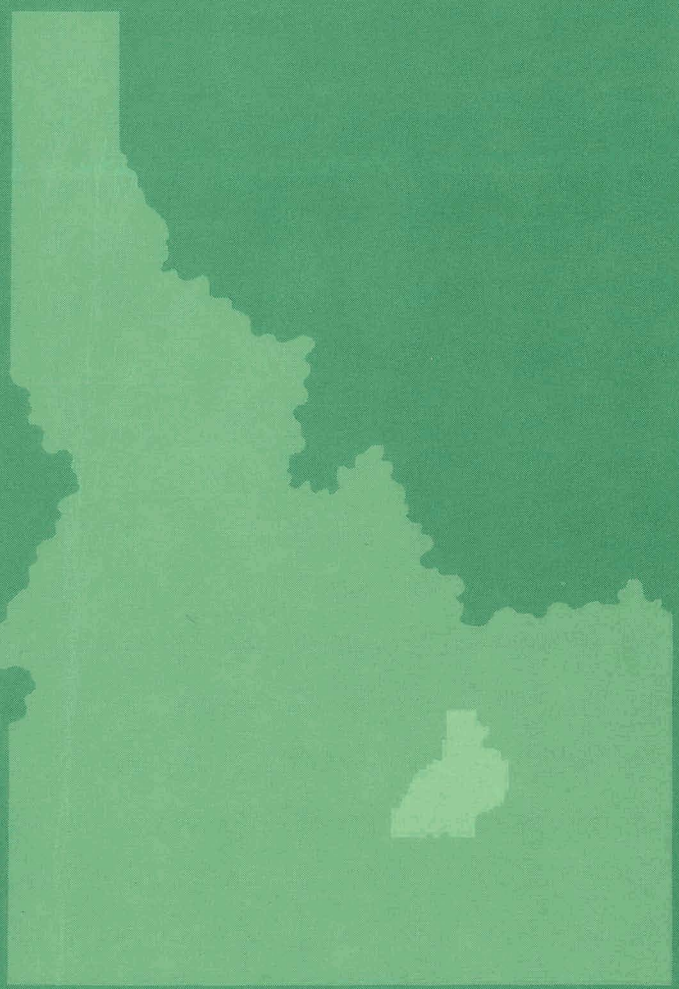

PHILLIPS PETROLEUM COMPANY

ATOMIC ENERGY DIVISION

NATIONAL REACTOR TESTING STATION

US ATOMIC ENERGY COMMISSION

DISCLAIMER

PRINTED IN USA. PRICE $2.00. AVAILABLE FROM THE CLEARINGHOUSE FOR FEDERAL SCIENTIFIC AND TECHNICAL INFORMATION, NATIONAL BUREAU OF STANDARDS U. S. DEPARTMENT OF COMMERCE, SPRINGFIELD, VIRGINIA

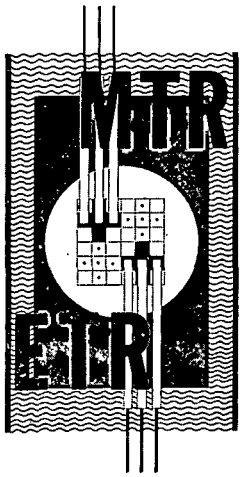

IDO-17147
AEC Research and Development Report
Reactor Technology
TID-4500
Issued: April 1966

NUCLEAR TECHNOLOGY BRANCHES QUARTERLY REPORT

FORMERLY -- MATERIALS TESTING REACTOR-ENGINEERING TEST REACTOR TECHNICAL BRANCHES QUARTERLY REPORT

JULY 1 - SEPTEMBER 30, 1965

D. R. deBoisblanc
ASSISTANT MANAGER
ATOMIC ENERGY DIVISION

W. C. Francis
MANAGER,
REACTOR ENGINEERING

R. G. Fluharty
MANAGER,
NUCLEAR TECHNOLOGY

PHILLIPS
PETROLEUM
COMPANY

Atomic Energy Division
Contract AT(10-1)-205
Idaho Operations Office
U. S. ATOMIC ENERGY COMMISSION

Previous Quarterly Reports in the MTR-ETR Series

Quarter	Number	Quarter	Number
	1959		1960
1	IDO-16543	1	IDO-16633
2	IDO-16561	2	IDO-16648
3	IDO-16580	3	IDO-16658
4	IDO-16620	4	IDO-16665
	1961		1962
1	IDO-16695	1	IDO-16781
2	IDO-16710	2	IDO-16805
3	IDO-16733	3	IDO-16827
4	IDO-16760	4	IDO-16857
	1963		1964
1	IDO-16898	1	IDO-16994
2	IDO-16917	2	IDO-17042
3	IDO-16932	3	IDO-17052
4	IDO-16977	4	IDO-17081
	1965		
1	IDO-17104		
2	IDO-17140		

SUMMARY

Repeated measurements, conducted over a period of two years, on a selected ETR fuel element have shown that the overall reproducibility of boron assays in the ETRC is 0.0274 g.

Irradiation of fuel and cladding materials specified for the ATR in a loop facility in the ETR at conditions prototypical of the ATR have shown apparent satisfactory fuel stability and aluminum corrosion rates in agreement with those measured in an ex-reactor loop.

Reduction in corrosion of ATR aluminum fuel plates by electroless nickel coating is being attempted. The nickel coatings showed no significant weight changes after corrosion testing in an autoclave at 350 to 400°F for 61 days. Under dynamic corrosion testing at 325°F and 25 ft/sec, the heat-treated, nickel-coated samples showed superior corrosion resistance to the as-plated specimens.

Out of five samples of electroless nickel coatings plated on 6061 aluminum alloy, only one showed diffusion to have occurred as a result of heat treatment. A microprobe study made on this sample revealed three distinct diffusion zones in the heat-treated condition.

An electron microscope examination of electroless nickel coatings on aluminum fuel plates showed a good bond was obtained when the aluminum base was roughened by pickling and the aluminum-nickel composite was heat treated for 40 hours at 400°C.

A preliminary comparison of the inelastic scattering in liquid lead yields qualitative agreement with a model that incorporates the idea of high-frequency collective modes of vibration. Detailed analysis is continuing.

Studies were made of geometrical effects in boron trifluoride neutron detectors in a preliminary study of the effects of electric field inhomogeneity on pulse-height response.

Void effects measurements designed to evaluate the reactivity worth of displaced water in the ARMF I showed (a) that reactivity worths of aluminum and water in the center location were not significantly affected by sample geometry over a large range of sample sizes and (b) that in the corner location, sample geometry effects were significant, but not large.

The swelling of Be samples cut from MTR lattice piece LB-15, which had been irradiated to 4.0×10^{21} fast n/cm^2 and containing 8.0 cc He/cc Be, is reported.

An upper limit of $\approx$ 1 millibarn was measured for the thermal neutron capture cross section of Be-10.

The alpha spectrum of Ac-227 chemically separated from Pa-231 is shown.

The sample holder for preparing and mounting wafer-thin radioactive samples for neutron cross-section experiments is described.

A number of computer programs were developed and written for the IBM 040 during this period.

Preparation continued for replacement of the IBM 1401 by the CDC 3100.

CONTENTS

FIGURES

TABLES

I. REACTOR ENGINEERING

1. CRITICAL FACILITIES
(E. E. Burdick)

Reproducibility of Boron Measurements in the ETRC (R. E. Oswald, A. D. Mackley)

Since early ETR operation, ETR fuel elements have been assayed in the ETRC to determine the effective built-in natural boron content. This report deals specifically with reproducibility errors in the boron assay values. Systematic errors are not treated because of lack of sufficient information at this time. The assaying technique is described in detail in a previous publication[1]; but in essence, it consists in establishing a calibration curve relating the effective boron of a test element to the position of a shim rod which is used as a measuring scale. In February 1963, one element (E298 A) was selected for use as a standard for long-term surveillance of the reproducibility of boron assaying results. In the two years that followed, the effective boron in E298A was measured 64 times. A standard deviation, σ_r (overall reproducibility), of 0.0274 g was obtained.

The 64 boron measurements on E298A were distributed through 12 boron assaying periods, each period requiring the establishment of a new calibration curve because of core changes that had occurred since the previous period. Because of the experimental error in establishing each new calibration curve, the measured boron values differed, on the average, from one curve to another curve. As a result, the overall standard deviation is larger than for a set of measurements which are all taken with the use of a single calibration curve. A more detailed analysis shows that the standard deviation, σ_m, for measurements using one curve is 0.0215 g.

From the data above, the standard deviation, σ_c, for the reproducibility of a point on the calibration curve (accuracy of the curve) may be computed. It is related to σ_r and σ_m through the relation

$$\sigma_r^2 = \sigma_c^2 + \sigma_m^2 \quad .$$

From this relation, $\sigma_c = 0.017$ g is obtained.

2. ENGINEERING EXPERIMENTS
(V. A. Walker)

Controlled Irradiation Testing of Uranium-Aluminum Fuels for the ATR (V. A. Walker, E. H. Porter, G. W. Gibson, M. J. Graber, M. Zukor)

The fuel material selected for the ATR core fuel elements represented an extension of the technology used successfully in the MTR and ETR. However, as shown in Table I-1, the operating conditions of the fuel elements in the ATR are somewhat more severe. Consequently, it has been necessary to conduct a

TABLE I-1

OPERATING PARAMETERS FOR
FUEL ELEMENTS IN MTR, ETR, AND ATR

Parameter	MTR	ETR	ATR
Maximum Nominal Heat Flux (Btu/ft^2-hr)	0.8×10^6	1.3×10^6	2.0×10^6
Thermal Power Density MW/ℓ (max nom.)	0.75	1.2	2.0
Maximum Nominal Fuel Plate Surface Temperature at Beginning-of-Life (°C)	115	165	180
Fuel Element Materials			
Cladding	1100 Al	1100 Al	6061 Al
Fuel Core	18 wt% U-Al alloy	22 wt% U-Al + 0.1 wt% B alloy	41 wt% U_3O_8 + + 0.2 wt% B_4C + Al cermet

series of irradiation tests to establish the suitability of the fuel element materials. The results of the first of these tests[2] indicated that the reference fuel material, U_3O_8 in X-8001 aluminum cermet, might not be suitable since extensive blisters were formed between 0.7×10^{21} and 1.0×10^{21} fiss/cc. The actual temperatures achieved by the samples were poorly defined since the increase in aluminum oxide thickness by corrosion of the cladding during irradiation was an unknown variable. The present work was undertaken to determine the stability of the reference fuel material and to study the cladding corrosion under carefully controlled and monitored conditions of irradiation.

Accordingly, a moderately pressurized water loop was designed, constructed, and installed in the G-12 position of the ETR core. To provide conditions prototypical of the ATR, a side stream of ETR primary coolant was pressurized to about 475 psig, and its pH adjusted to 5.0 ± 0.2 by nitric acid addition prior to its passage through the fueled channels at a velocity of about 46.5 fps. A schematic diagram of this loop is shown in Figure I-1.

The conditions achieved during the irradiation are shown in Table I-2. All of the fuel materials performed satisfactorily from a stability viewpoint at exposures of up to 2.0×10^{21} fiss/cc. It was found that the measured in-pile corrosion of the 6061-0 aluminum cladding determined by instrumented fuel plates agreed reasonably well with that predicted from a correlation developed from ex-reactor experiments[3]. The formation of the adherent alumina corrosion film, such as the one shown in Figure I-2, appears to limit the usefulness of 6061-0 aluminum alloy as a result of thermally induced stresses and the marked decrease in alloy physical properties with increasing temperature above about 175°C.

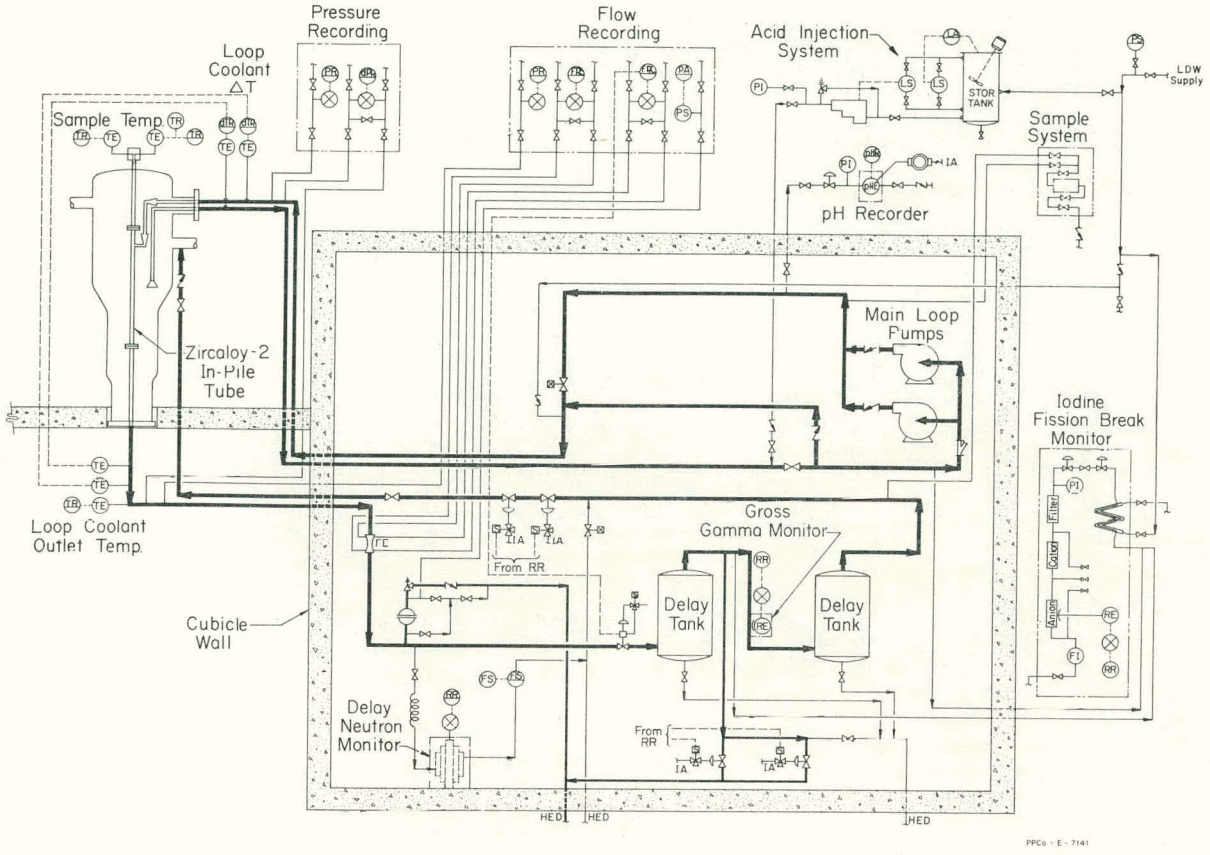

Fig. I-1 Layout of G-12 loop at ETR.

TABLE I-2

SUMMARY OF IRRADIATION CONDITIONS AND RESULTS FOR ATR FUEL MATERIALS

Fuel Material[a]	Maximum Nominal Beginning-of-Life Surface Temperature (°C)	Maximum Nominal Beginning-of-Life Surface Heat Flux (10^6 Btu/hr - ft^2)	Calculated Maximum Nominal Cladding-Oxide Interface Temperature (°C)	Fission Density (10^{21} fiss/cc)	Measured Maximum Alumina Thickness (mils)
41 wt% U_3O_8 + 0.19 wt% B_4C	160	2.0	240	1.9	1.2
50 wt% UAl_3 + 0.19 wt% B_4C	160	2.0	240	1.9	1.3
Spherodized Cb-coated 35 wt% UO_2 + 0.19 wt% B_4C	170	2.2	270	2.0	2.1[b]
41 wt% U_3O_8	150	1.4	180	1.1	1.0
55 wt% UAl_3 + 0.19 wt% B_4C	140	1.7	160	1.5	1.0

[a] Fuel matrix was X-8001 aluminum alloy, and cladding material was 6061-0 aluminum alloy in all cases.

[b] This value is probably not representative since upstream plate was found warped following irradiation which may have changed channel velocity and operating wall temperatures downstream.

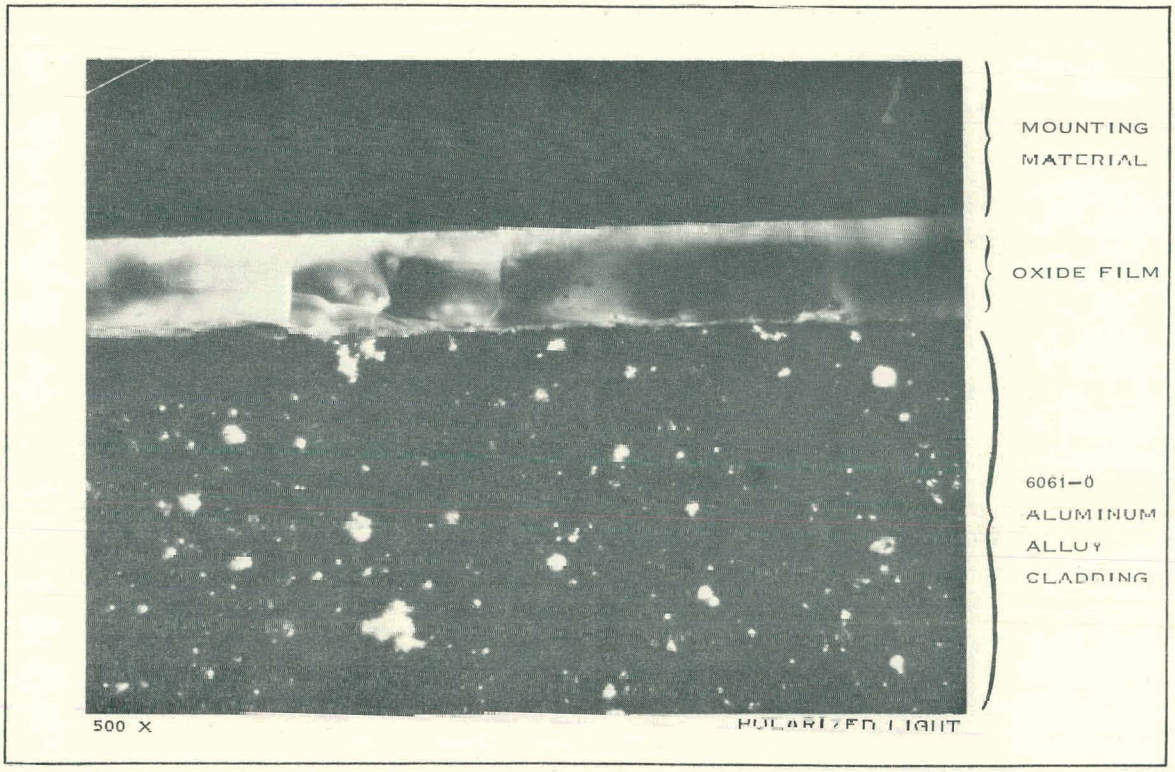

Fig. I-2 Microstructure of ATR sample fuel plate showing oxide film on surface.

Several methods of reducing or eliminating the oxide film are being investigated, including the use of electroless nickel coatings which have been successfully used at Hanford[4].

3. METALLURGICAL DEVELOPMENT
(G. W. Gibson)

Electroless Nickel Plating (M. Zukor, B. G. Carlson, G. W. Gibson)

During the second ATR fuel irradiation program in the ETR, it was noticed that under ATR conditions, a corrosion deposit built up on the surface of the aluminum fuel plates (previous section). This deposit acts as a thermal barrier, increasing plate temperatures. One approach to eliminating this problem is to coat the surface of the aluminum fuel plate with a thin layer of nickel.

The most promising method for nickel coating aluminum fuel plates appears to be by use of an electroless nickel-plating process[5]. This process consists of the reduction of a nickel solution with hypophosphite ion. When a catalytic surface, such as aluminum, is immersed in this plating solution, a uniform nickel coating plates out on the metal surface. An amorphous, high nickel-low phosphorus alloy is deposited, the reactions being[6,7]:

$$Ni^{++} + H_2PO_2^- + H_2O \xrightarrow[\text{Catalyst}]{\text{Heat}} Ni^0 + H_2PO_3^- + 2H^+$$

$$3Ni^{++} + H_2PO_2^- + 7H\cdot \xrightarrow[\text{Catalyst}]{\text{Heat}} Ni_3P + 5H^+ + 2H_2O$$

$$2H^+ \xrightarrow{\text{Catalyst}} 2H\cdot \rightarrow H_2\uparrow .$$

Upon heat treatment, diffusion occurs, and the nickel coating exhibits several diffusion zones. Microprobe analyses are given in the next section of these diffusion zones.

Several Ni-coated Al plates were corrosion-tested in an autoclave at a pressure of 125 to 200 psig and temperatures of 350 to 400°F for periods up to 61 days. Table I-3 shows the weight changes. The as-plated, Ni-coated, 6061 Al plate had a 3/16-inch unplated border along one edge, and it is this

TABLE I-3

AUTOCLAVE CORROSION TESTING
OF ELECTROLESS Ni-COATED Al PLATES

	Description	Time in Autoclave (days)	Weight Change (mg)
6061 Al Control	6061 T-6 condition (bare)	37	-202.1
1100 Al	PPCo Ni-coated 1100 Al HT: 40 hours at 400°C	61	+ 1.9
6061 Al	PPCo Ni-coated 6061 Al HT: 40 hours at 400°C	61	- 1.7
APM-M-257 Al	PPCo Ni-coated APM-257 Al HT: 40 hours at 400°C	61	- 3.8
6061 Al	ORGDP Ni-coated 6061 Al As-plated (3/16-inch unplated border along one edge)	61	-13.1

exposed Al which accounts for the small weight change. This plate was Ni coated at the Oak Ridge Gaseous Diffusion Plant. No significant weight changes were noted for the Ni-coated specimens after 61 days; whereas, the uncoated 6061 Al control plate lost 202 mg after only 37 days.

Six electroless Ni-coated plates of 6061, 1100, and APM-M-769 aluminum alloys with various heat treatments were corrosion-tested in the Reactor

Engineering Corrosion Loop at 163°C and 25 ft/sec. Figure I-3 plots the results of this test. The results confirm the fact that heat treatment of the Ni coatings significantly reduces the corrosion rate [8].

Presently, Ni-coated, 6061 Al plates are undergoing corrosion testing at 191°C and 45 ft/sec in the Reactor Engineering Corrosion Loop. Ni-coated plates are also under irradiation in the L-51 position of the MTR. Further testing of heat-treated, Ni-coated, 6061 Al plates is scheduled for irradiation under ATR conditions in the G-12 position of the ETR.

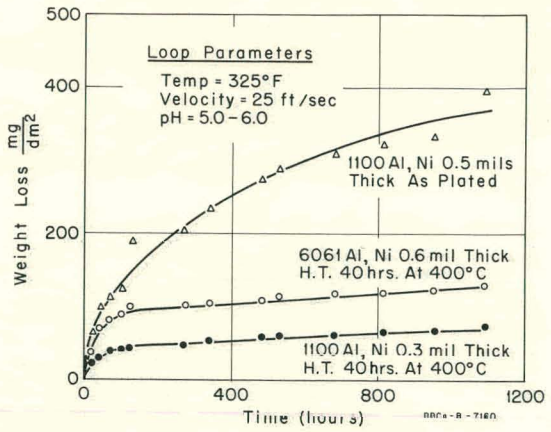

Fig I-3 Corrosion rates of electroless nickel-plated aluminum alloys.

4. MATERIALS RESEARCH
(J. M. Beeston)

4.1 Electron Microprobe Examination of Electroless Ni Coatings on 6061 Aluminum Alloy (W. F. Zelezny)

Five samples of the electroless nickel coatings plated on 6061 aluminum alloy, as discussed elsewhere in this report, were examined by means of the microprobe to ascertain the distribution of several elements within the nickel plating before and after heat treatment. Only one of these samples showed diffusion to have occurred as a result of the heat treatment. The results of the examination of one specimen are given in detail by means of illustrations, and the results obtained from the other specimens are summarized in tabular form.

One specimen (Sample No. 1002) was subjected to a temperature of 450°C for 36 hours. The photomicrographs and microprobe chart recordings in Figures I-4 and -5 show that appreciable diffusion across the Al-Ni boundary has taken place, resulting in the formation of four distinct regions within the nickel coating. The microprobe chart recordings reproduced in Figure I-4 reveal that the outermost region (Region A) contains no aluminum while the aluminum concentrations are approximately constant within each of two regions (Regions C and D) but differ from one region to the other. The aluminum content appears to vary continuously across Region B.

A scan for P and Si was made across the coating on this same plate as illustrated in Figure I-5. The phosphorus is revealed as ranging across most of the two outer layers, with its highest concentration at or near the interface between these layers. The silicon occupies a narrow band immediately inward from and partially overlapping the phosphorus distribution. The peak silicon concentration occurs at or near the boundary between Regions B and C.

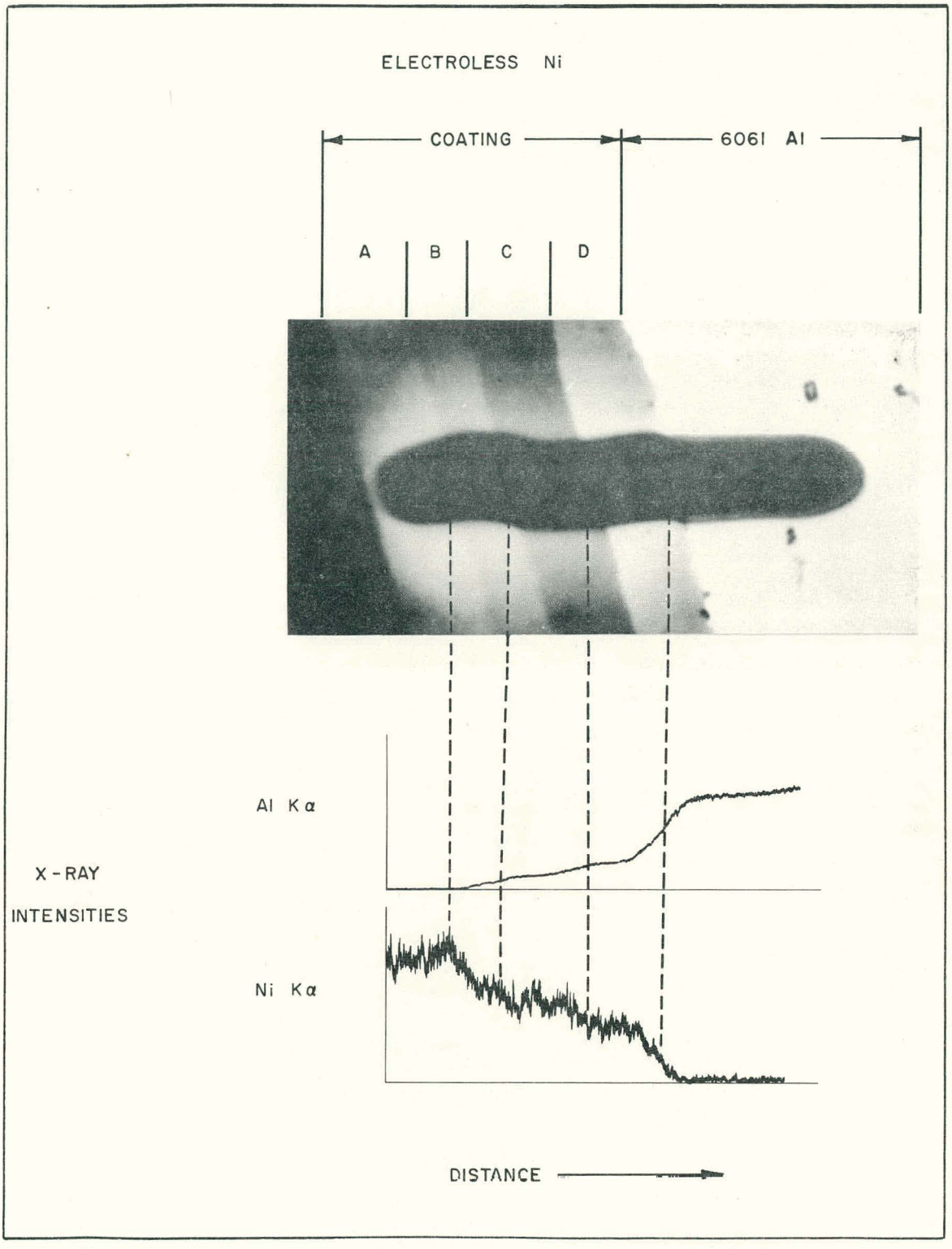

Fig. I-4 Microprobe scan showing relative intensity of Al and Ni in nickel-coated 6061 Al sample which was heat treated at 450°C for 36 hours.

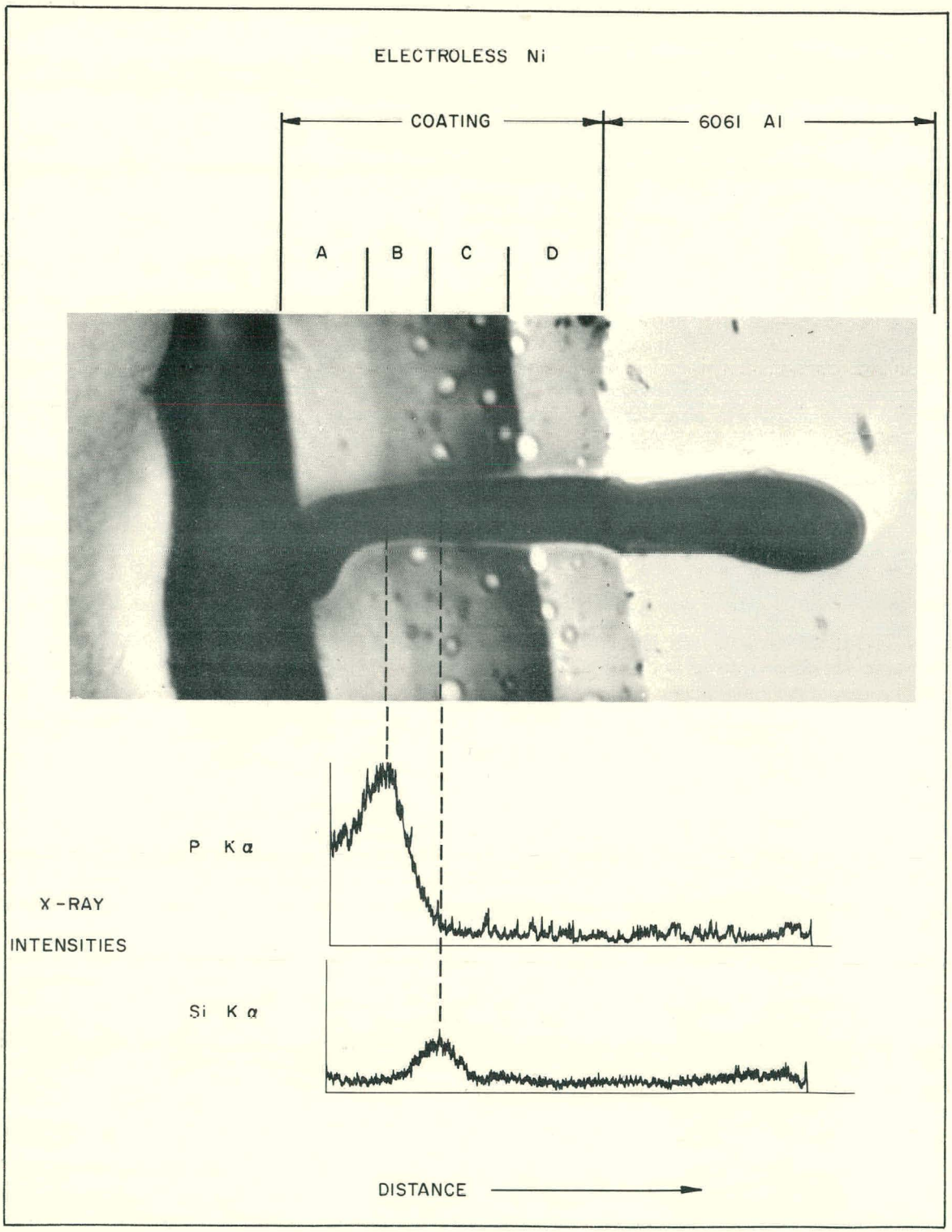

Fig. I-5 Microprobe scan showing relative intensity of P and Si in nickel-coated 6061 Al sample which was heat treated at 450°C for 36 hours.

Another plate (Sample 1026) was likewise examined both before and after heat treatment at 450°C for 20 hours. The coating on this plate before heat treatment showed a slight tendency to split into two layers of equal thickness. After heat treatment, splitting was found in a number of places. This tendency to split was attributed to the fact that the plating process was interrupted overnight and resumed the next day. The microprobe showed uniform concentrations of nickel, copper, and phosphorus entirely across the coating both before and after heat treatment and in both parts of the coating where it had split.

The results are summarized in Table I-4. Except for the first plate mentioned, only doubtful indications of silicon, with no tendency for the silicon to concentrate in any region, were found.

TABLE I-4

SUMMARY OF RESULTS OBTAINED BY MICROPROBE EXAMINATION OF ELECTROLESS NICKEL COATINGS ON 6061 Al ALLOYS

Sample Source and Identification Number	Heat Treatment	Results Shown by Microprobe Examination
PPCo 1002	36 hours at 450°C	See Figures I-4 and -5. Pronounced interdiffusion of Al and Ni, giving four distinct layers. Outer layer is Ni containing some P. Inner layers contain Al, increasing inward toward 6061 Al base. P is concentrated near boundary between outermost Ni layer and adjoining Ni-Al layer. Narrow band of high Si immediately inside region of P concentration.
PPCo 1026	None	Ni, Cu, and P uniform throughout coating. Slight tendency of Ni layer to split into two layers. No diffusion between Al and Ni.
PPCo 1026	20 hours at 450°C	Splitting of Ni layer in some regions. Concentrations of Ni, Cu, and P uniform throughout both split and unsplit portions of coating. No diffusion between Al and Ni.
ORGDP[a] 1019	None	Ni, Cu, and P uniform throughout coating. No diffusion of Al and Ni.
ORGDP	1-1/2 hours at 485°C	Interdiffusion of Al and Ni beyond resolution limit of microprobe. P is essentially uniform throughout coating, with occasional indications of slightly higher P in a narrow band in coating immediately adjoining underlying 6061 Al.

[a] Oak Ridge Gaseous Diffusion Plant.

4.2 Electron Microscopy of Electroless Nickel Coatings (R. A. Moen)

Electron microscopy was performed on several of the electroless nickel-coated aluminum plates cleaned (pickled) by different processes and on heat-treated plates.

Figure I-6 represents the 6061 aluminum-nickel interface in the as-plated condition (ORNL complex acid pickle). Figure I-7 also illustrates a 6061 aluminum-nickel interface, the aluminum having been pickled in a chromic acid solution. Figure I-8, an APM 769 aluminum plate coated with nickel and subsequently heat treated for 40 hours at 400°C, shows evidence of three distinct diffusion zones. Fuel plates, coated and heat treated for two hours at 400°C, do not show a detectable diffusion zone.

The enhanced corrosion resistance of the nickel-coated aluminum fuel plates depends on the adherence of the thin nickel film. The type of nickel-aluminum interface shown in Figure I-6 provides a better mechanical bond than the interface

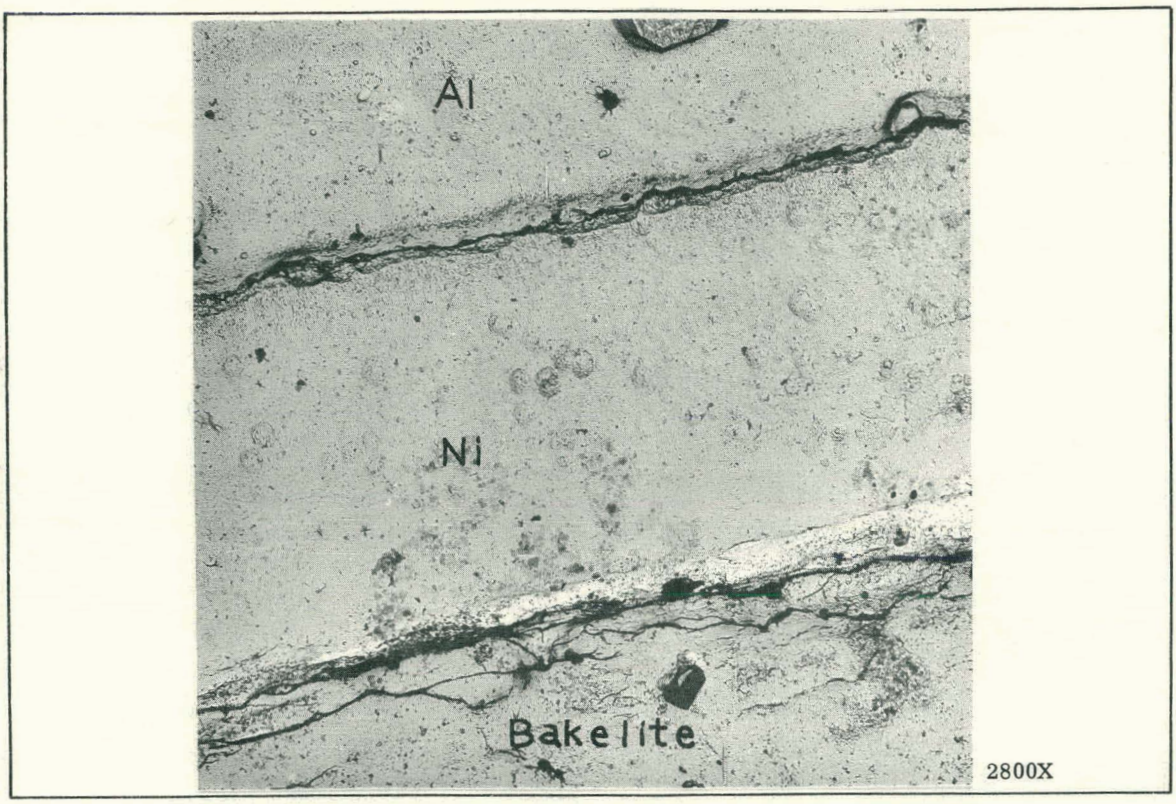

Fig. I-6 Electroless nickel coating on 6061 Al, as-plated, pickled in complex acid.

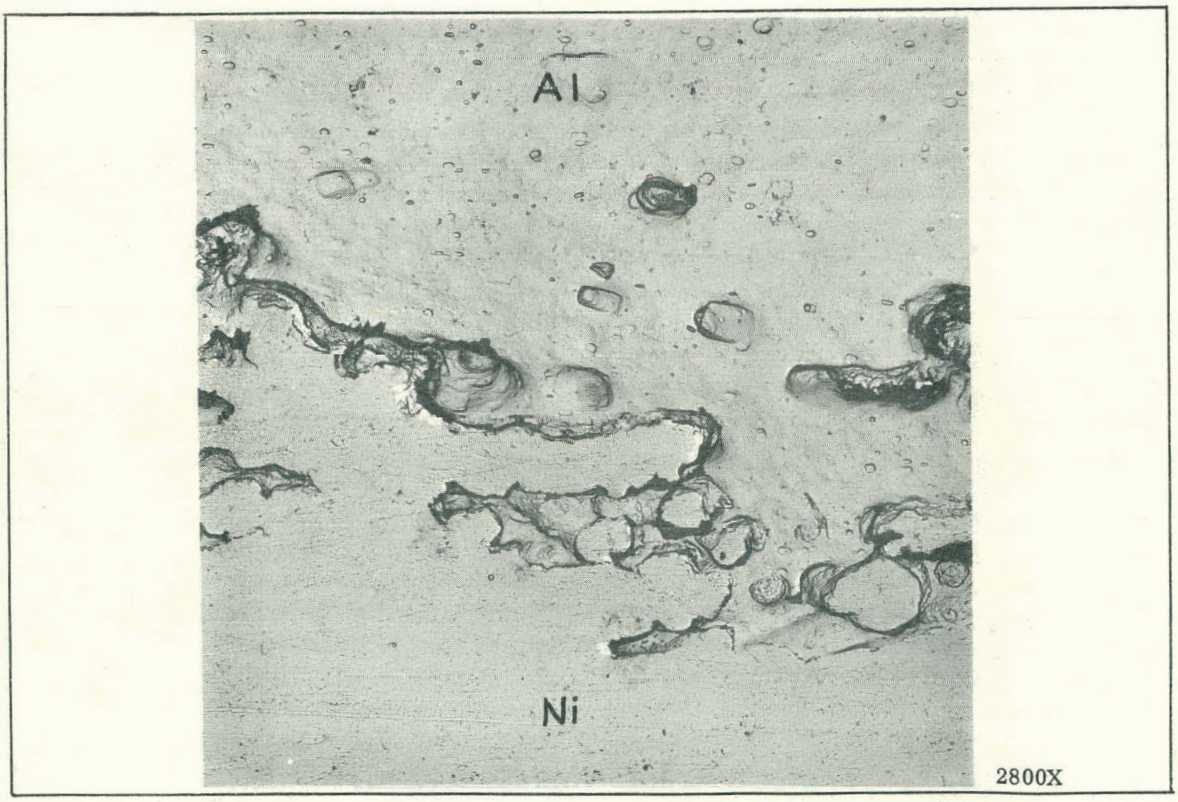

Fig. I-7 Electroless nickel coating on 6061 Al, as-plated, pickled in chromic acid.

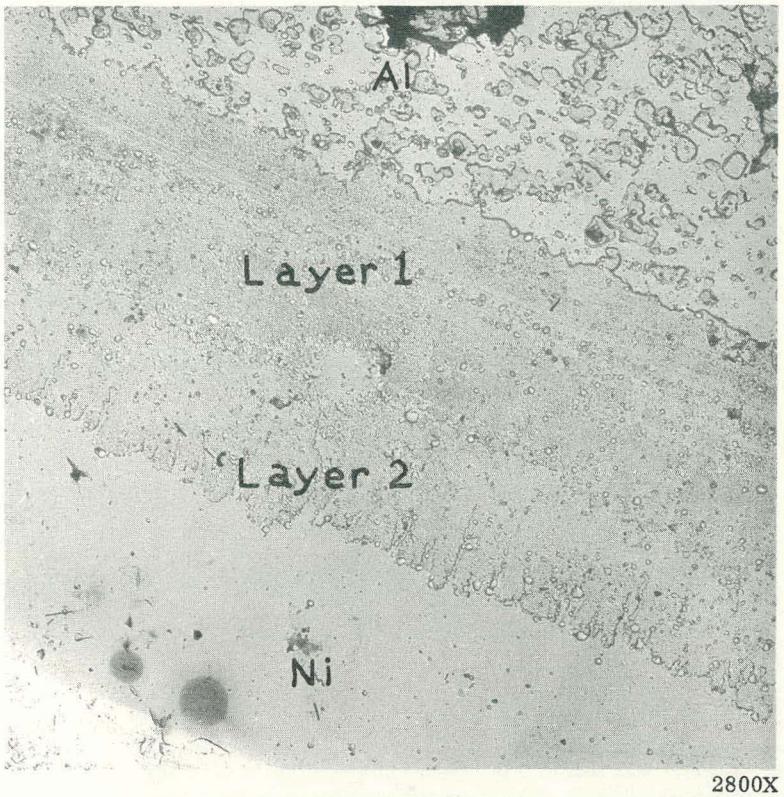

Fig. I-8 Electroless nickel coating on APM 769 Al, heat treated 40 hours at 400°C.

shown in Figure I-7. Comparing Figures I-7 and -8, it can be seen that the heat treatment has provided a diffusion bond between the aluminum and nickel. The combination of a roughened aluminum surface from pickling prior to nickel plating and a subsequent heat treatment has produced a coating with good adhering appearance.

5. REFERENCES

1. J. W. Henscheid, "Fuel Element U-235 and Boron Content Analysis", Quarterly Progress Report for MTR-ETR Technical Branches, First Quarter - 1958, IDO-16474 (September 1958) p 14.

2. W. C. Francis, V. A. Walker, and G. W. Gibson, "High-Temperature Irradiation Testing of Uranium/Aluminum Fuels for the ATR", ANS Transactions, 6, No. 2 (November 1963) p 373.

3. J. C. Griess, H. C. Savage, and J. L. English, Effect of Heat Flux on the Corrosion of Aluminum by Water, Part IV. Tests Relative to the Advanced Test Reactor and Correlation with Previous Results, ORNL-3541 (February 1964).

4. A. B. Johnson, Jr., Behavior of Chemical Nickel Plate on Aluminum Alloys in High Temperature, Dynamic, Aqueous Systems, HW-81196 (April 1964).

5. G. Gutzeit and E. T. Mapp, " 'Kanigen' Chemical Nickel Plating", Corrosion Technology, 3, No. 10 (October 1956) pp 331-336.

6. K. T. Ziehlke, W. S. Dritt, and C. H. Mahoney, "Heat Treating Electroless Nickel Coatings", Metal Progress, 77 (February 1960) pp 84-87.

7. A. W. Goldenstein et al, "Structure of Chemically Deposited Nickel", J. Electrochem. Soc., 104 (February 1957) pp 104-110.

8. A. B. Johnson, Jr., Behavior of Chemical Nickel Plate on Aluminum Alloys in High Temperature, Dynamic, Aqueous Systems, HW-81196 (April 1964).

II. NUCLEAR TECHNOLOGY

1. CROSS SECTIONS
(M. S. Moore)

1.1 An Evaluation of a Square BF_3 Neutron Detector (G. E. Stokes)

A series of tests was run to compare a square BF_3 neutron detector with a round BF_3 neutron detector. The square BF_3 tubes were tested to see if they were satisfactory for use on the MTR Fast Chopper. If they performed well, they would be used to provide a uniform detector in the beam for time-of-flight measurements. The tube tested was a Reuter-Stokes model No. SK-162. Its overall length was 22 inches with an 18-inch active length. It was a 1-inch square tube filled with boron trifluoride to a pressure of 65 cm Hg. The anode was 0.006 inch in diameter, and the tube had a 0.032-inch aluminum wall. The filling pressure, center wire diameter, and wall thickness were the same as our present round BF_3 tubes.

The tests were run on the MTR crystal spectrometer with the tube positioned in the Bragg beam. The arm was positioned to give a maximum counting rate with a minimum gamma-ray background. The beam was collimated with 0.040 inch of cadmium to a slit approximately 1 inch high and 0.050 inch wide. This beam struck the tube as shown in Figure II-1. The tube was shielded from background until a signal-to-noise ratio of about 400:1 was achieved. The tube was mounted on a translational table and positioned such that the first reading was taken at the outside edge of the tube. Thus, the outside edge gave a micrometer reading of 0 while the center of the tube was 0.500 inch. The micrometer was advanced in 0.050-inch steps, and a series of voltage settings was run for each step. The data were recorded in a 256-channel, pulse height analyzer with the discriminator set at 0 so the whole input pulse was recorded. A round BF_3 counter was set up under the same conditions to give a comparison with the square tube.

A pulse response as a function of distance from the edge of the tube for the square tube is shown in Figure II-2. It should be noted that the pulse height spectrum changes as the edge of the tube is approached.

Figure II-3 shows the effects of voltage on the pulse height response of the square tube. The change in response due to position is similar to the response due to a change in voltage. This would indicate that there is a pronounced voltage nonuniformity as the edge of the tube is approached. Figure II-4 shows the round BF_3 tube's neutron response as a function of position, and Figure II-5 is the same tube at a given setting with the voltage being varied.

It appears that the square BF_3 counter is not an acceptable detector for use on the fast chopper. There is no clear point to discriminate against the gamma noise without losing a significant number of neutron counts. The two peaks that appear as the voltage is changed are both neutron response peaks. Further study of these response effects may give a better understanding of the BF_3 detection process. Because the present measurements show this tube to be unsatisfactory, a jitter time measurement was not attempted.

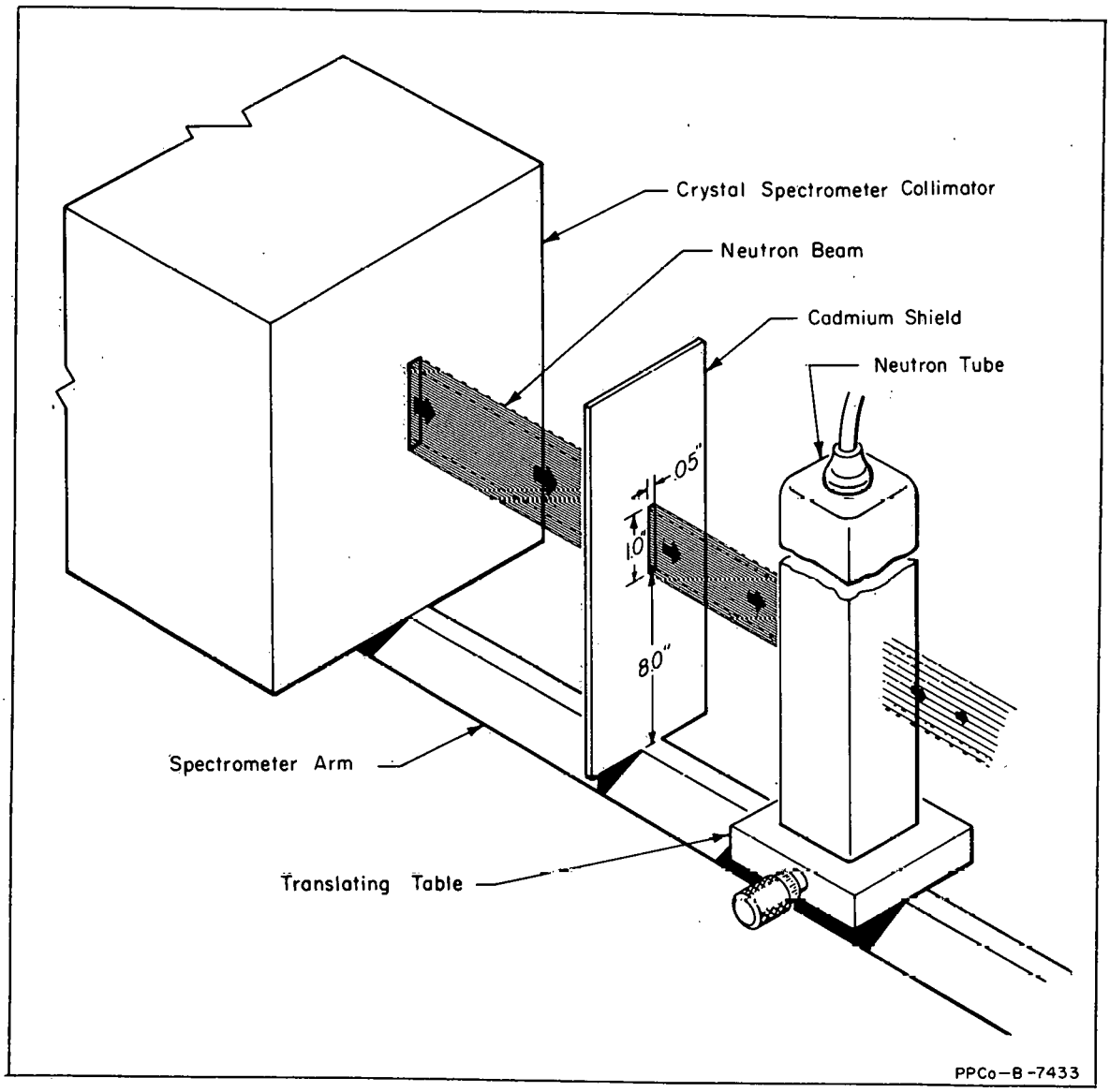

Fig. II-1 The neutron beam is shown striking the tube. It should be noted the beam covers a very small section of the detector tube. The translating table allows the tube to be moved across the beam for various data positions.

1.2 Total Neutron Cross Section of Tc-99 (T. Watanabe)

Total cross-section measurements of Tc-99 from 0.02 to 200 eV have been made with sample thicknesses of 44, 72, 180, and 1090 barn/atom. Resonances observed at 5.65, 20.29, 39.868, and 56.42 eV are undergoing area analysis to obtain parameters. Since the p-wave strength function (size resonance curve) has a peak in the region of A = 100, the data are also being examined for p-wave resonances.

1.3 Total Neutron Cross Section of Pu-242 (T. E. Young)

A PuO_2 + Al pressed sample containing 700 mg of PuO_2 enriched to 99.88 percent in Pu-242 has been used to measure the total cross section of Pu-242 from 0.008 to 1000 eV. With a sample thickness of n = 0.00370 atoms/barn and

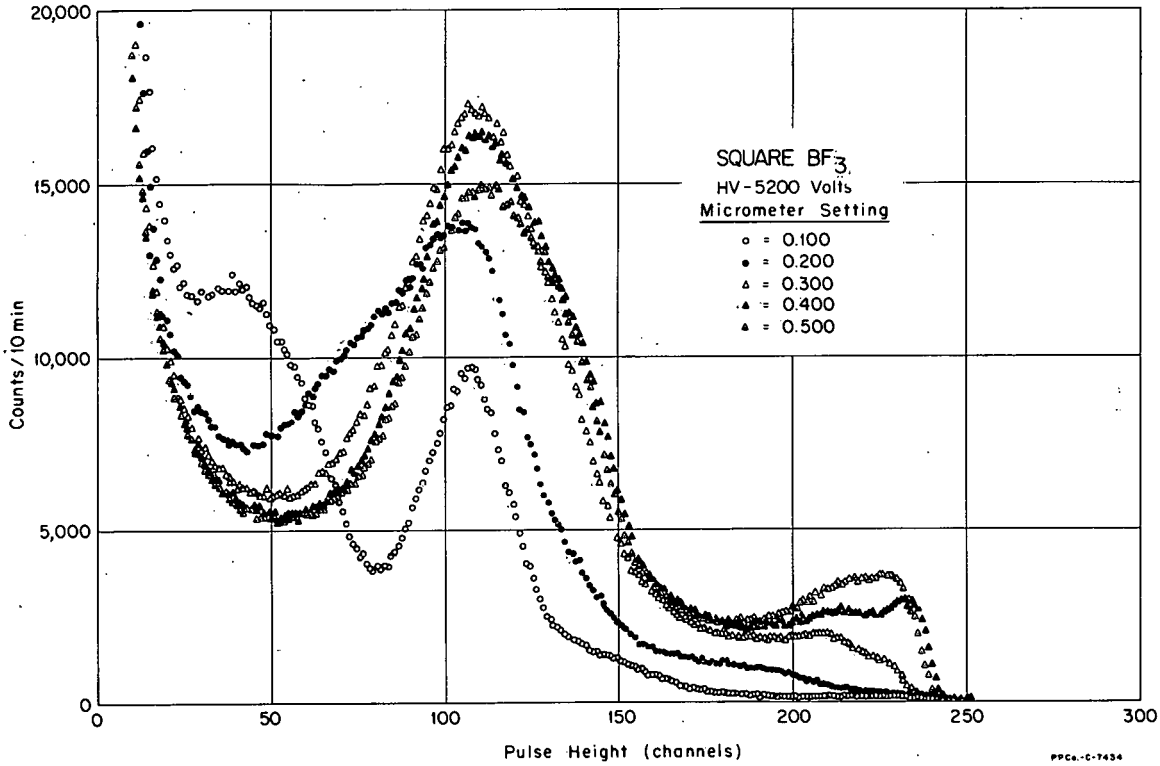

Fig. II-2 A square BF_3 tube showing a plot of pulse height spectra as a function of distance from the edge of the tube. A micrometer reading of 0.00 is the extreme edge and 0.50 is the center of the tube.

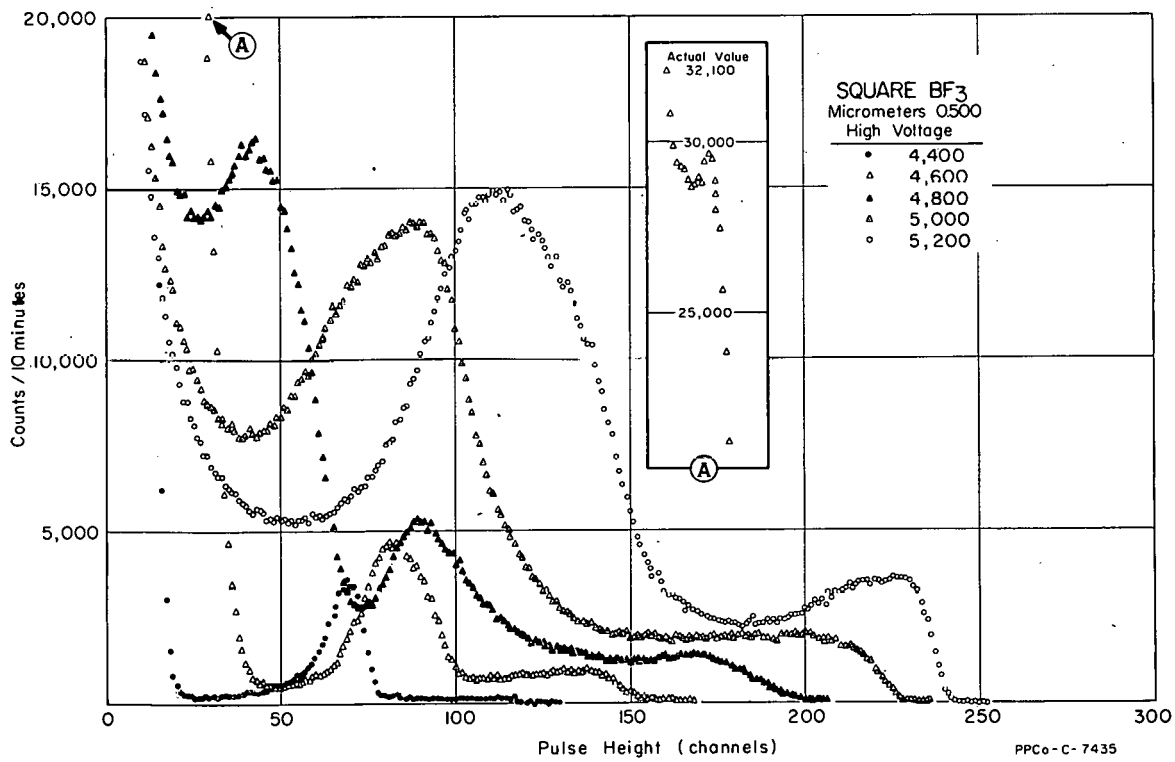

Fig. II-3 A square BF_3 tube showing a plot of pulse height response as a function of voltage applied to the tube. Note the movement of the two peaks in the response as a function of voltage.

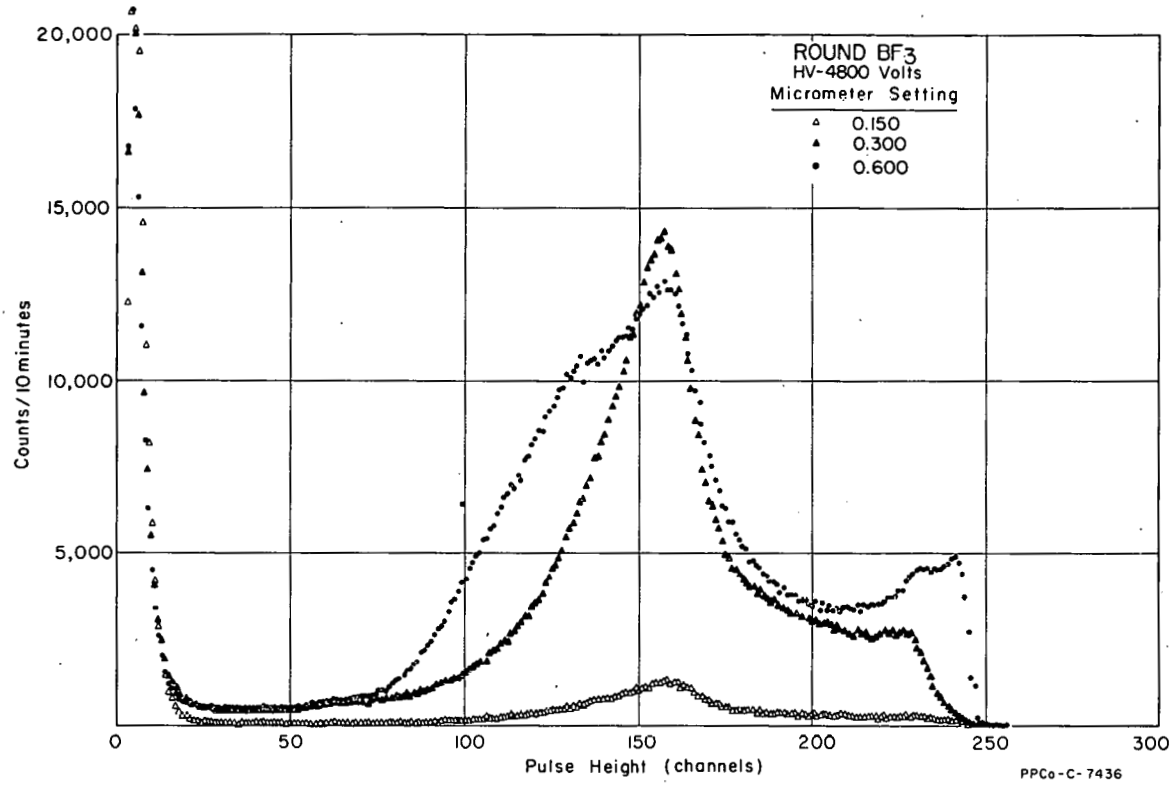

Fig. II-4 A round BF_3 pulse height response as a function of distance from the edge of the tube. A micrometer reading of 0.00 is the edge and 0.50 is the center.

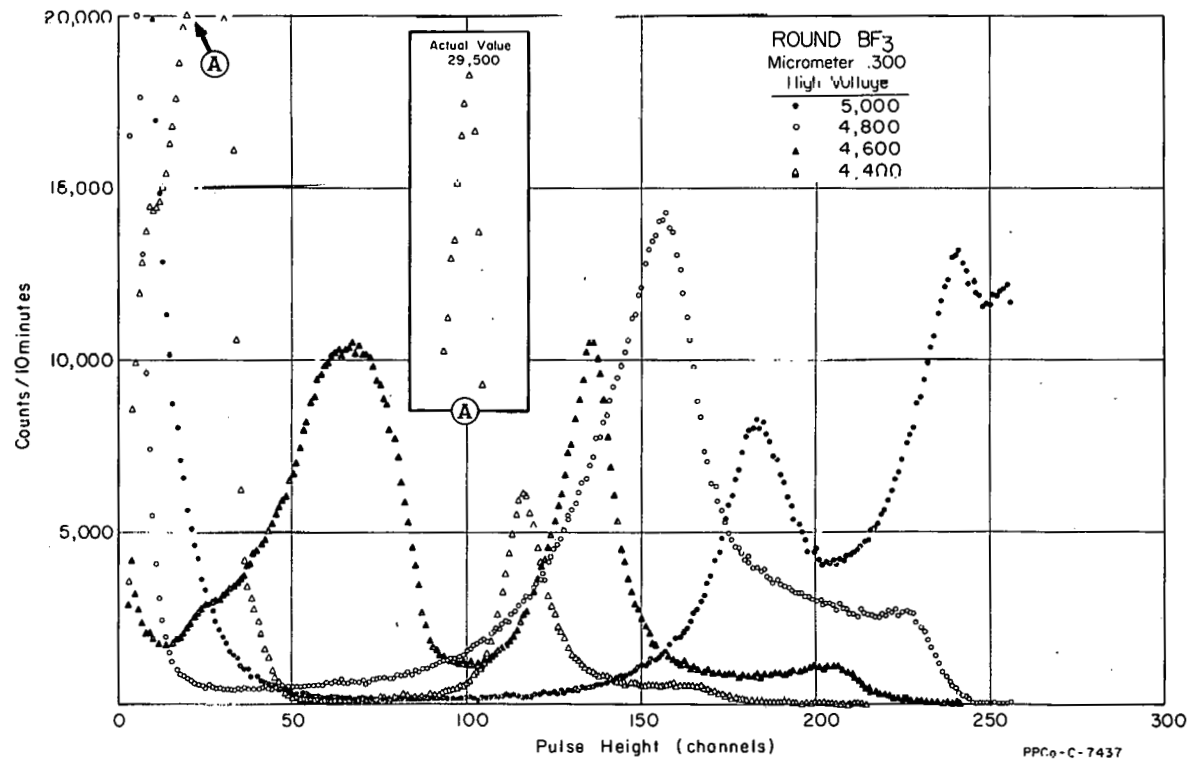

Fig. II-5 A round BF_3 pulse height response as a function of voltage applied to the tube.

an instrument resolution of 0.1 μsec/meter, resonances were observed at the following energies:

22.6 ± 0.2 eV[a]	
41.0 ± 0.6 eV[a]	
53.6 ± 0.8 eV	
67.9 ± 1.2 eV[a]	
107 ± 2.0 eV[a]	
132 ± 3.0 eV[a]	
150 ± 4.0 eV[a]	
207 ± 6.0 eV[a]	
321 ± 12.0 eV[a]	

Measurements with lower resolution showed the known resonance at 2.68 ± 0.02 eV, and gave a 2200 m/sec cross section of 39 ± 1 barns.

2. NUCLEAR CHEMISTRY
(W. H. Burgus)

2.1 Swelling of Irradiated Beryllium (R. L. Tromp)

During the quarter, experiments were completed on the swelling of Be samples cut from MTR lattice piece LB-15 which had been irradiated to 4.0×10^{21} fast n/cm^2 and contained 8.0 cc He per cc Be. The irradiation had been carried out at MTR ambient temperature; and after sectioning samples with an underwater abrasive cutoff wheel, the sectioned samples were heated in vacuo at various temperatures for varying periods of time. Rates of evolution of gas were determined along with irreversible changes in density. Earlier experiments with Be with this gas content (8.0 cc/cc Be) were reported for heating temperatures of 500 and 600°C[1]. With the completion of this phase of the project, another point has been added to the beryllium swelling threshold curve.

The density versus heating-time behavior of five separate samples is shown in Table II-1 and plotted in Figure II-6.

The irreversible swelling threshold temperature is ≈ 650°C. Rates of gas evolution are plotted in Figure II-7. In Figure II-8, a plot of swelling threshold temperature versus fast (> 1 meV) neutron dosage is shown, and it can be seen that the point at 8.0 cc He/cc Be falls quite well on the curve drawn through swelling threshold temperatures for gas contents well above and below this value.

2.2 The Neutron Capture Cross Section of Be-10

Attempts were made to determine the thermal neutron capture cross section of Be-10 by activation to Be-11. Irradiated Be which contained ≈ 500 ppm Be-10

[a] Not previously reported

TABLE II-1

DENSITY VERSUS HEATING-TIME BEHAVIOR OF FIVE SAMPLES

Cumulative Heating Time (hr)	Density (g/cm^3)				
	500°C	600°C	650°C	700°C	800°C
0	1.8608	1.8302	1.8290	1.8205	1.8424
1	---	---	---	1.7767	1.6247
2	1.8526	1.8457	1.8311	1.7371	1.5224
4	---	---	---	1.6169	1.4678
6	1.8457	1.8524	1.7662	---	---
8	---	---	---	1.5901	1.4436
12	1.8470	1.8122	1.6961	1.5857	1.3925
20	1.8419	1.8267	---	1.5772	---
30	---	1.8001	---	---	---

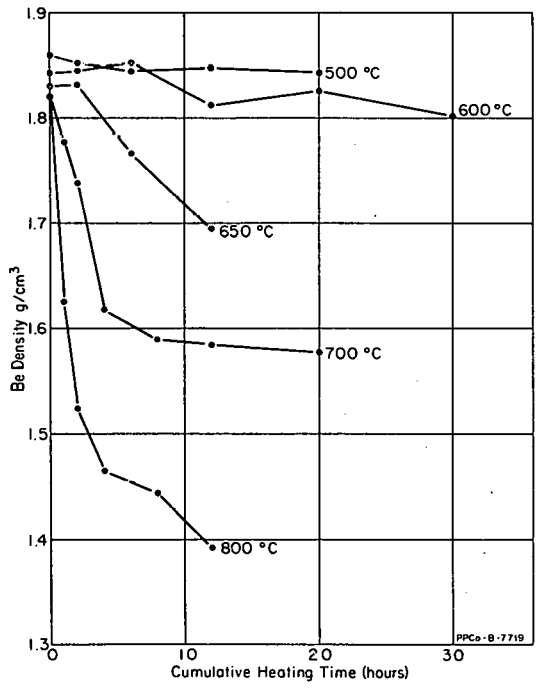

Fig. II-6 Density versus heating time of irradiated Be.

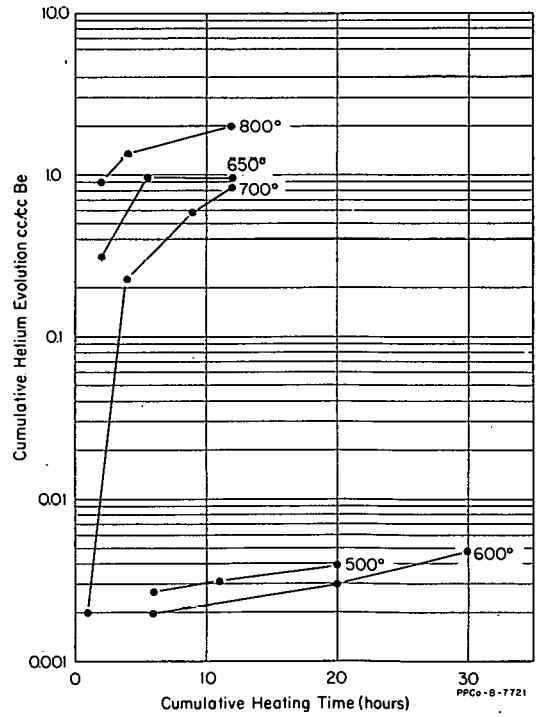

Fig. II-7 Rates of gas evolution from irradiated Be.

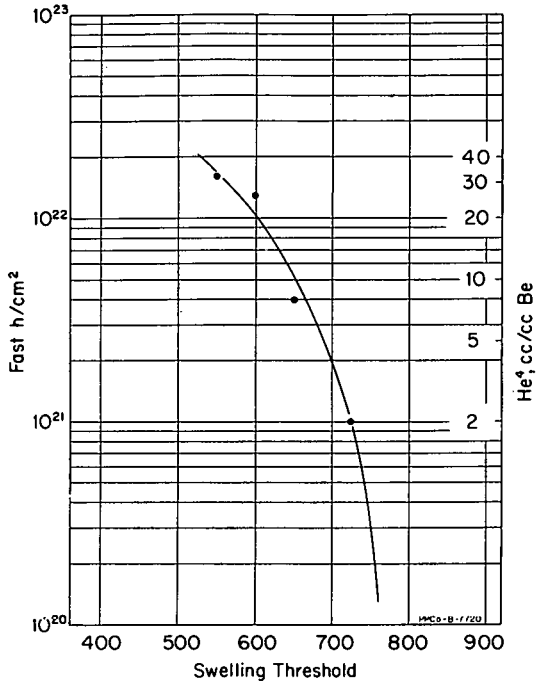

Fig. II-8 Swelling threshold temperature versus fast neutron dosage.

was radiochemically purified until no observable gamma-emitting impurities were present. The material was converted to oxide and re-irradiated to Be-11 saturation in the VG-7 pneumatic rabbit facility in MTR. After this re-irradiation, the material was examined with the aid of sodium-iodide scintillation spectrometer, looking for the 2.11 MeV γ-ray of Be-11. Gamma radiation of this energy was barely discernible over a background of Al-28 radiation arising from inert Al-27 impurity in the sample. In two runs, cross-section values of 4.8 and 5.2 x 10^{-4} barns were calculable from the sketchy data, but pending better purification of the material to be re-irradiated, an upper limit of only $\approx$ 1 millibarn may be quoted at this time. More precise values may be obtained upon removal of Al impurity and by use of higher flux irradiations.

2.3 Alpha Spectrum of Ac-227 (R. N. Chanda, R. A. Deal)

Alpha spectrum studies of the Pa-231 natural decay chain have continued. Ac-227 has been chemically isolated and its alpha spectrum observed on a gold-surface barrier detector (Figure II-9).

The following chemical procedure was used to isolate the actinium from other members of the Pa-231 chain: A solution of Pa-231 and its daughters in 6M HCl-1M HF was evaporated to dryness and taken up in 2M HNO_3. In order to remove Pa-231, three solvent extractions were made with a 30 percent solution of Aliquat-336 in benzene. Following a benzene wash, the Th-227 was extracted from the aqueous phase with a 1.5M solution of bis (2 ethyl-hexyl) phosphoric acid (EHPA) in kerosene. After adjusting the aqueous phase to pH 2, a second EHPA extraction carried the Ac-227, isolating it from Ra-223. The Ac-227 was back extracted with 2M HNO_3, and a final extraction made with Aliquat-336 to ensure complete separation from Pa-231 and also to remove Po, Bi, and Pb.

As can be seen from Figure II-9, there are at least seven alpha lines corresponding to the following energies: 4.95, 4.94, 4.87, 4.85, 4.79, 4.76, 4.73, and 4.70 meV. These lines are in agreement with the work of Novicova et al [12]; however, no evidence for a line which they report at 4.52 keV has been seen. According to the Russian work, this line should appear with an intensity equal to one-half the 4.70 meV line intensity and, thus, should have been readily observable in our work. In addition, we observe weak lines at 4.43, 4.58, and 4.60 meV not reported in the Russian work. These lines are as yet unassigned.

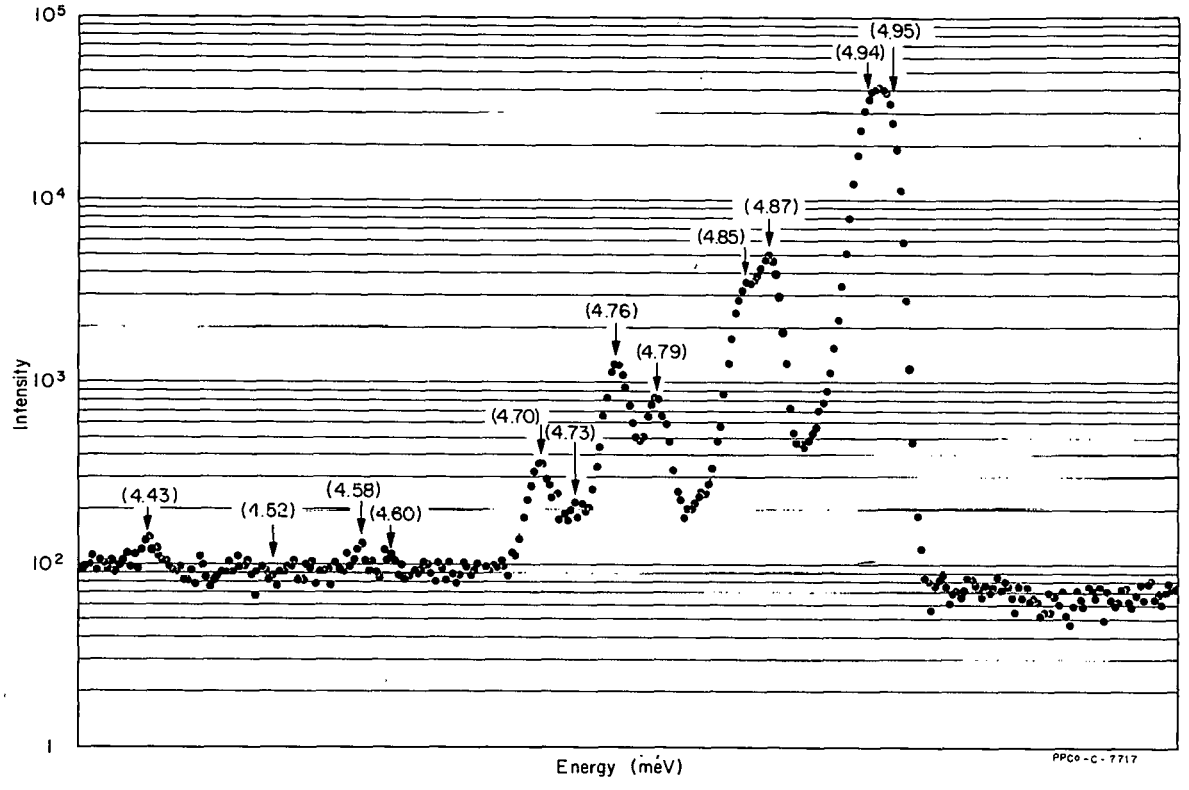

Fig. II-9 Alpha Spectrum of Ac-227.

2.4 Fabrication of Wafer-Thin Radioactive Samples for Los Alamos Cross-Section Experiments (J. R. Berreth)

Collaborative participation in the Los Alamos cross-section experiments using neutrons produced from underground bomb shots has resulted in considerable design work toward fabricating suitable target samples. The proposed experiments will be conducted mostly with highly radioactive isotopes. This fact plus the unique character of the neutron source necessitates that certain requirements be met. Primary considerations for the sample are that it be of sufficient size to intercept the entire neutron beam so total cross section measurements may be conducted; that it be sufficiently thick to cause an observable change in transmission for most resonances over a wide energy range; further, that since the neutron source is available for only a very short period of time (and only once for each experiment), the sample should ideally consist only of the desired material or, at most, a minimum amount of "inert" matter; finally, that the sample must be tightly contained because of potential radioactive contamination considerations.

Consistent with the above requirements, developmental methods of fabrication have been investigated. The present plans are to use the oxide of the desired material (perhaps mixed with a minimum of aluminum as a binder) and press it directly into a retaining ring which has very thin (1 mil or less) nickel windows. The resultant wafer would be approximately 10 mils thick. Figure II-10 shows a tentative design for a sample holder incorporating the above features. The holder consists of two iron rings, each having a thin nickel window soldered to it. The lower ring acts as the die for compacting the sample.

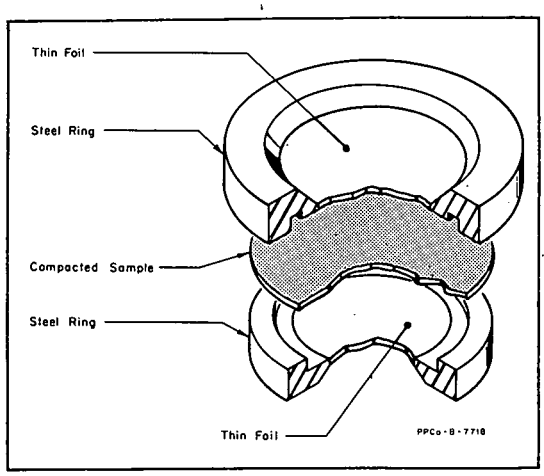

Fig. II-10 Sample holder for Los Alamos cross-section measurements.

The upper ring serves as the compacting punch and also seals the pressed sample at the same time by means of an interference fit around the outside of the lower ring. Both rings are backed up with auxiliary punches while pressing. Samples so produced are approximately 1.5 inches in diameter and will be placed at 45-deg angles to the beam, thus allowing ideal detector arrangements.

Preliminary tests have shown that compaction is satisfactory without a binder. A serious flaw at present is that the oxide wafer buckles upon removal from the press. This may be caused by mismatching of the backup punches to the rings or expansion of the rings under pressure. Expansion is less likely since only 30,000 psi is used in pressing. A lower pressure may eliminate the problem. Tests have not been performed as to the leak tightness of the closed rings.

2.5 Fabrication of Fast Chopper Samples

The method of fabricating radioactive samples for use on the Fast Chopper is being reappraised. The compacts presently in use have at times been broken. Less frequent breakage has been encountered upon removal from the dies than when handling with manipulators. In order to eliminate breakage, pressing of the sample material directly into a container has been studied. This method is much more difficult for our purposes; and in determining accurately the sample cross-sectional area, it may have a slight disadvantage. Choice of proper container material and die arrangement along with the envisioned lower pressure used in compacting should minimize any error due to expansion. Above all, the fabrication of samples should be more reliable, and much less breakage should be encountered.

The fabrication of the long narrow rectangular slot (0.055 by 1.089 inches) can only be accomplished by electrical discharge machining. Two test containers have been fabricated and have proved the feasibility of the machining. The special retaining die is now in the design stage.

3. INELASTIC SCATTERING
(R. M. Brugger)

Liquid Lead (P. D. Randolph)

A preliminary analysis of the liquid lead data that were obtained last quarter has been completed. This analysis was done in terms of a model proposed by Singwi[3] for the coherent scattering in liquids. The model is an attempt to improve the convolution approximation for coherent scattering which was first proposed by Vineyard[4]. It assumes that outside a "coherence

radius" R (≈10 to 20 Å) the convolution approximation is valid and that, inside this radius, the liquid can support high-frequency collective oscillation or quasi-phonon excitations for times of the order of 10^{-12} sec. The atoms inside this sphere are treated in the single-phonon harmonic approximation.

The one-phonon result for the reduced partial differential cross-section form of the scattering law $S_{Rcoh}(\kappa,\omega)$ has the form,

$$S_{Rcoh}(\kappa,\omega) = S_{Rinc}(\kappa,\omega)\left[1 + \gamma(\kappa) + \frac{\omega^2}{6c^2} L(R,\kappa,q)\right] \quad (1)$$

and is restricted to the inelastic scattering, ie, $\hbar\kappa^2 D \ll \hbar\omega \ll 2k_B T$. Here, $\hbar\kappa$ and $\hbar\omega$ are the neutron momentum and energy transfer, respectively; $1 + \gamma(\kappa)$ is the liquid structure factor (obtained from diffraction experiments); c is the velocity of sound in the liquid; $L(R,\kappa,q)$ is the correction to the convolution approximation; q is the wave vector magnitude of the quasi-photon excited in the liquid; D is the macroscopic coefficient of self-diffusion; and T is the sample temperature. In this model, the one-phonon incoherent scattering law is given by

$$S_{Rinc}(\kappa,\omega) = \left(\frac{\sigma_{coh}}{4\pi\, k_B T}\right) \frac{\hbar^2\kappa^2}{2M\, k_B T}\, e^{-2W}\, \frac{f(\omega)}{\omega^2} \quad (2)$$

where 2W is the Debye-Waller factor and $f(\omega)$ is the frequency spectrum which must be assumed for the liquid.

In the preliminary analysis reported here, experimental curves of $L(R,\kappa,q)$ have been obtained from smooth curves drawn through the experimental scattering law plots of $S_R(\kappa,\omega)$ versus κ at fixed ω. Figure II-11 shows some representative data plots of the scattering law. These are shown as a function of wave vector transfer, κ, at constant energy transfer, $\beta = [E-E_o]/k_B T$, where $k_B T = 54$ meV corresponding to a temperature, T = 625°K (350°C). Each curve comprises data taken at three incident energies, 15, 17.5, and 20 meV. There has been no normalization applied to the three runs. These curves show the characteristic momentum dependent structure earlier observed in liquid sodium[5], but because of the higher intensity and improved energy and momentum resolution of this experiment, the structure is much better defined than in the sodium experiment. Also, the damping of this structure with increasing energy transfer is easily observed. It is one of the basic purposes of Singwi's model to explain this damping of the structure in the inelastic scattering.

To obtain the experimental $L(R,\kappa,q)$ curves, the data were corrected for multi-phonon excitations and for multiple scattering. The multi-phonon correction was calculated using the LEAP program of Egelstaff[6]. The frequency spectrum used for this and also for calculating the one-phonon $S_{inc}(\kappa,\omega)$ is the one proposed by Singwi for the phonon modes,

$$f(\omega) = \frac{4}{\omega_m^3}\, \omega^2\, e^{-2\omega/\omega_m} \quad (3)$$

The peak of this spectrum ω_m corresponded to a temperature T_m of 60°K (ie, $\hbar\omega_m \equiv k_B T_m$).

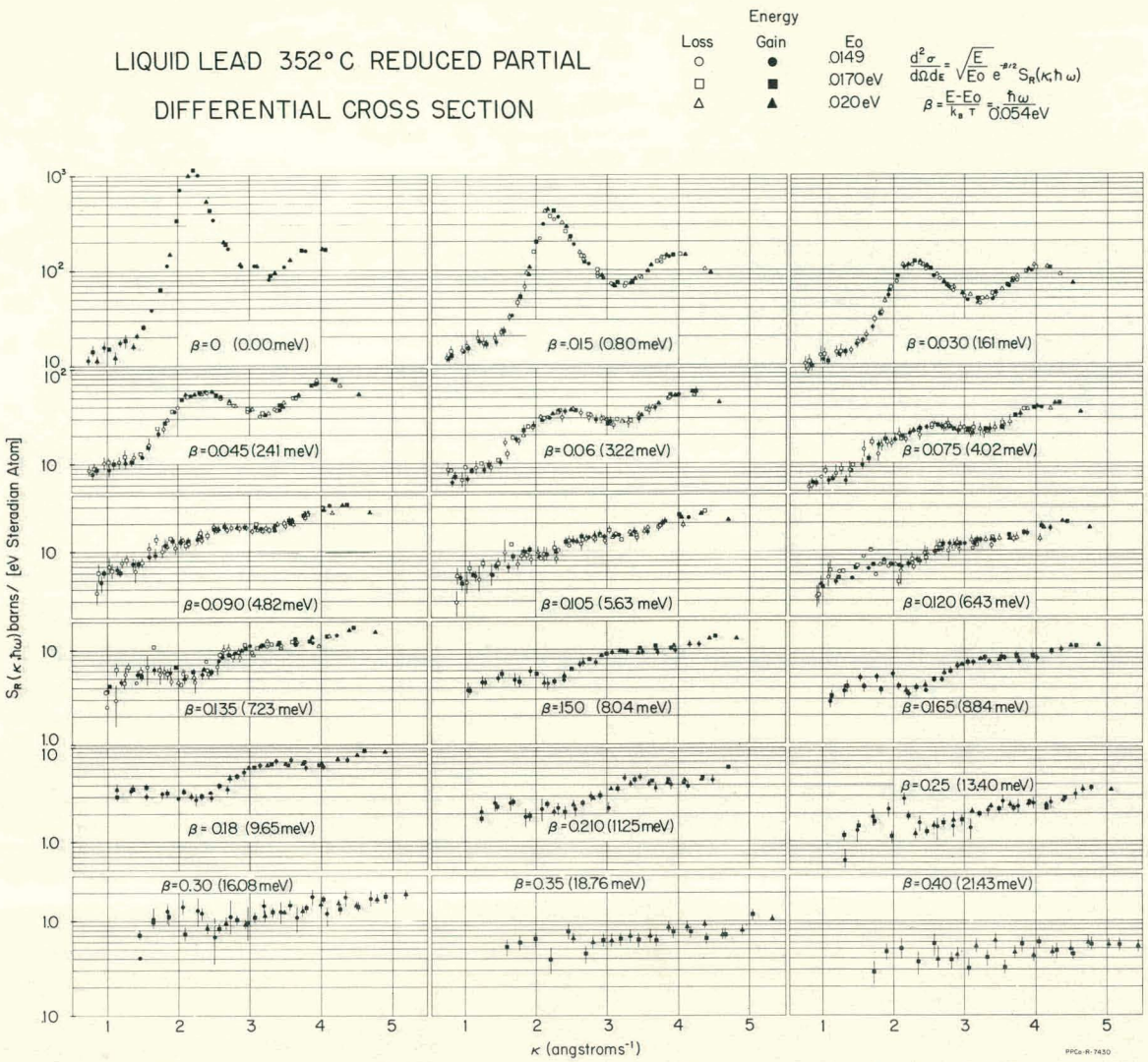

Fig. II-11 Curves of reduced partial differential cross section for liquid Pb.

The correction for multiple scattering is an estimated one. This estimate was made using the Placzek first-moment relation as a condition that the corrected scattering law should satisfy. In terms of the reduced partial differential cross section, this relation is given by the ratio,

$$A \frac{\langle \beta^1 \rangle}{\kappa^2} = 1$$

where

$$\langle \beta^1 \rangle = 2 \int_0^\infty \beta \sinh(\beta/2)\, S_R(\kappa,\beta)\, d\beta$$

and

$$A = \frac{8\pi M (k_B T)^2}{\sigma_b \hbar^2} \quad ; \quad \beta = \frac{\hbar\omega}{k_B T} \; .$$

The multiple scattering correction was assumed to be isotropic (ie, independent of κ). The β dependence of the multiple scattering was taken to be 80 percent of the uncorrected scattering law at $\kappa = 1$, the lowest value of κ reached in

the experiment. The wings of this curve were then adjusted until, on the average, the moment ratio was satisfied within about 30 percent. Without this correction, the ratio was as much as a factor of seven too large. Figure II-12 shows a plot of the ratio of the observed first moment to its theoretical value with and without the multiple scattering correction. As is seen from this plot, the moment ratio is only about half of its theoretical value, showing that at $\kappa=1$ the correction is too large. However, in spite of the crudity of the correction and the assumption that it is isotropic, the improvement in the moment ratio is quite marked.

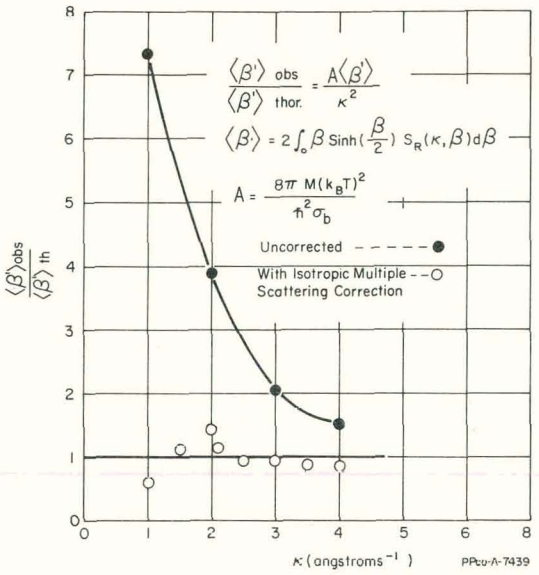

Fig. II-12 Ratio of observed to theoretical values of the first moment of the energy transfer for liquid Pb at 350°C, showing the effect of an isotropic correction for multiple scattering.

After correcting the observed scattering law for the above effects, an experimental $L(R,\kappa,q)$ was obtained using Equations (1), (2), and (3). For the structure factor $1 + \lambda(\kappa)$, the values obtained by Kaplow et al from X-ray diffraction [7] have been used. The velocity of sound was taken to be 2×10^5 cm/sec and independent of q. Such a straight line dispersion curve is in agreement with the measurements of Cocking and Egelstaff [8].

In Figure II-13 are shown some experimental curves of the correction function $L(R,\kappa,q)$ for different energy transfers, β. Also theoretical curves of $L(R,\kappa,q)$ are shown. The coherence parameter for the theoretical curves has been taken to be R = 20 Å. There are also shown a few points at small κ using a different multiple scattering correction. This correction assumed that the entire measured scattering law at $\kappa = 1$ is caused by multiple scattering, and no changes were made in the wings of this correction. The general effect was a 20 percent increase in the amplitude of the correction. The resulting effect on $L(R,\kappa,q)_{exp}$ is large, showing that L is very sensitive to this correction at small κ.

The minimum predicted by the theory is present in the experiment at the predicted κ value, but it is somewhat broader than predicted and is deeper. As β increases, the agreement in the depth of the minimum becomes better. The two positive maxima predicted by theory on either side of the minimum are present; however, the amplitude does not agree with the model. The disagreement is larger at small κ than at large κ. However, as we have seen, at small κ the experiment is very sensitive to the multiple scattering.

In general, the experiment and theory appear to agree in their basic features though there are discrepancies in details. It is concluded that the theoretical model which assumes that collective modes of vibration exist over a limited distance in the liquid, demonstrates most of the features observed in coherent scattering and, thus, constitutes a great improvement over the convolution approximation.

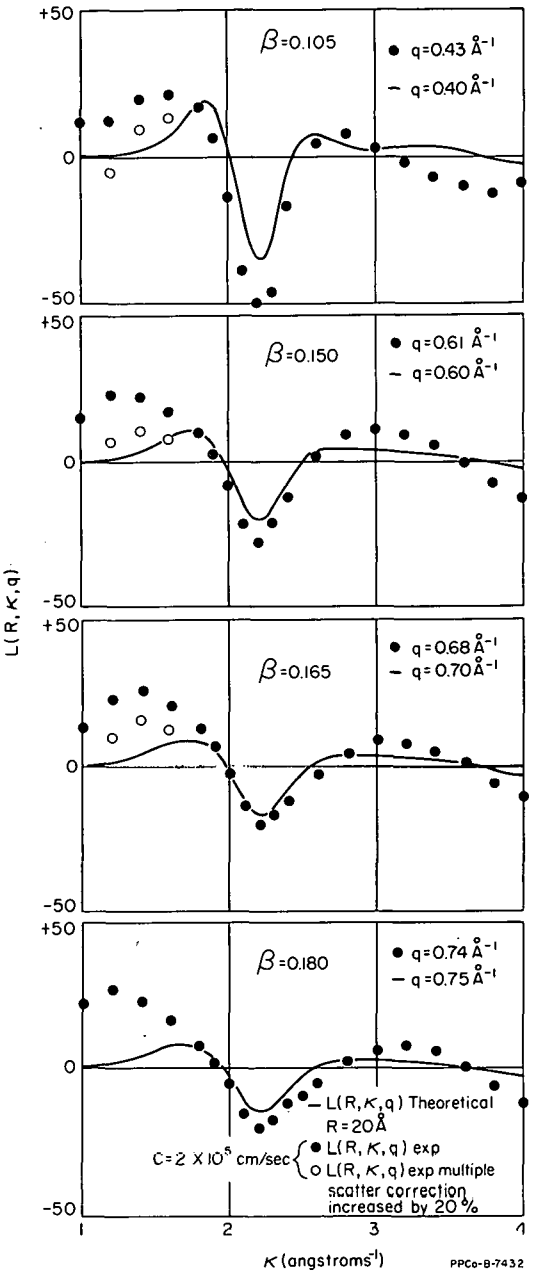

Fig. II-13 Comparison of experimental and theoretical curves of L(R, K, q), the correction to the convolution approximation, for liquid Pb at 350°C.

4. REACTOR EXPERIMENTS
(E. Fast)

Interpretation of Reactivity Measurements -- Void Effects (R. G. Nisle, J. W. Rogers)

4.11 Introduction. The reactivity of a small sample, as measured by the Advanced Reactivity Measurement Facilities, is a composite of several effects, due to changes in absorption, fission, scattering, moderation, or water displacement resulting from the introduction of the sample into the reactor. In any given sample, one or more of these processes may dominate; and in general, the sample is designed in such a way that the dominant process is the one of interest. In every case, however, water is displaced; and an attempt is made to account for that fact by the use of standard samples or "blanks", that is, samples of identical geometry containing no active materials. This procedure is satisfactory if the volumes of all samples are identical or if, in case of volume differences, the volume is directly related to weight and a weight correction is made. In any case, it is of interest to know the magnitude of the required volume correction. It is only on the basis of such knowledge that a sound judgement can be made as to the nature of the corrections that need to be made in any given case.

The present experiment was designed, therefore, to measure the reactivity worth of the water displaced for two sample types and to separate the effect of variations in sample weight from the effect of water displacement.

4.12 Description of Experiment. The two sample types are illustrated in Figure II-14. Each consisted of a hollow aluminum capsule with a watertight cap sealed with an O-ring. A sequence of aluminum sleeves of varying thickness was used to vary the weight. Reactivity measurements were made in the center and in a corner location in the ARMF I. Hence, for each sample type, there resulted a series of reactivity values as a function of sample weight at constant sample volume. A typical plot of one set of data is shown in Figure II-15.

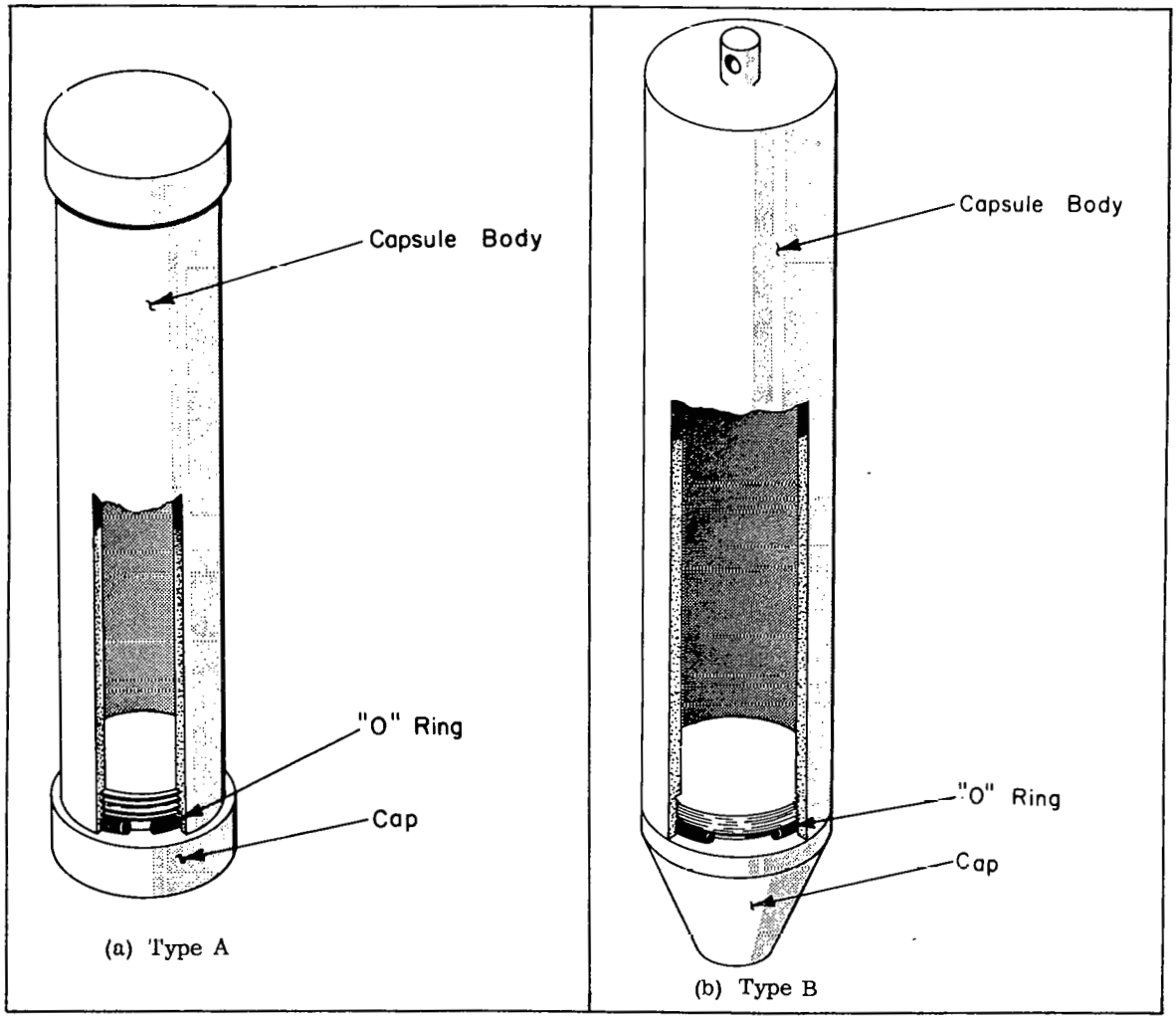

Fig. II-14 (a) Sample Type A
(b) Sample Type B

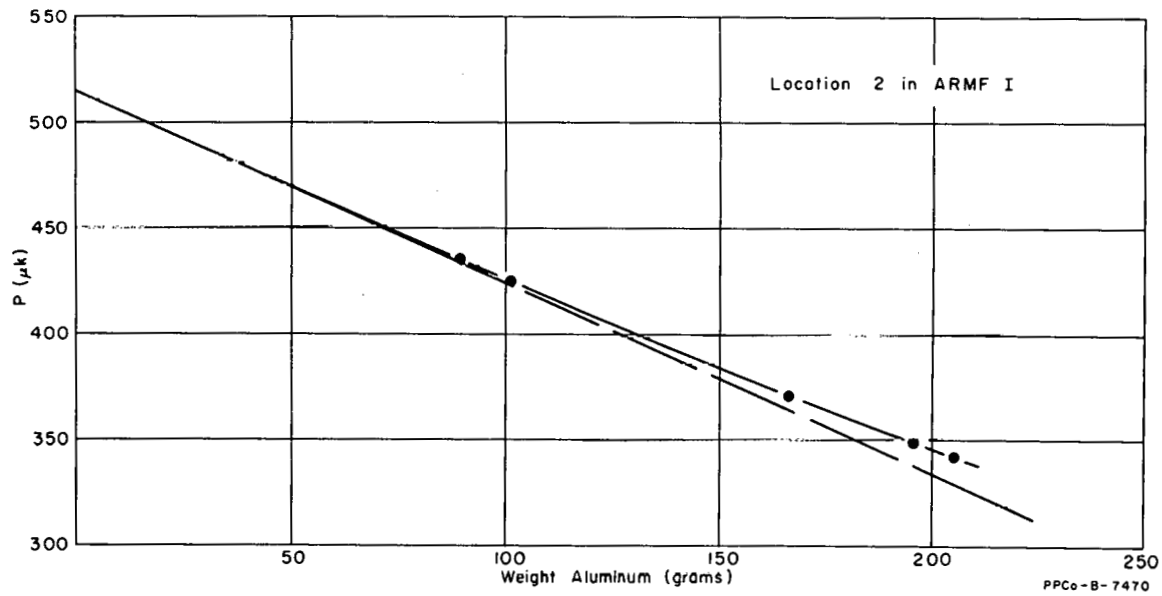

Fig. II-15 Sample plot of reactivity versus aluminum weight (capsule Type A).

A nonlinear, least-squares curve fitting computer program was used to fit the expression

$$\rho(W) = A + B\,W + C\,W^2$$

to the data. Then the value of $\rho(O) = A$ is the worth of the water displaced by the sample, and the value of

$$\left[\frac{d\,\rho(W)}{d\,W}\right]_{W=0} = B$$

is the worth of the aluminum in μk per gram at no self shielding. The worth of the water displaced, in μk per cc, may then be found by dividing A by the volume of the sample.

4.13 Results and Conclusions. The results are listed in Table II-2.

TABLE II-2

REACTIVITY WORTH OF
ALUMINUM AND WATER IN THE ARMF I

Sample Type	Location	Aluminum (μk/g)	Water (μk/cc)
A	Center	-0.549 ± 0.110	-4.278 ± 0.095
	Corner (Fig.. II-15)	-0.964 ± 0.076	-6.704 ± 0.066
B	Center	-0.530 ± 0.053	-4.294 ± 0.040
	Corner (sleeves)	-0.946 ± 0.007	-6.362 ± 0.005
	Corner (rods)	-0.862 ± 0.125	-6.311 ± 0.096

The agreement between the worth of aluminum for the two samples in the center location is seen to be within the quoted uncertainties. The same holds for the water worth in this location. In the corner location, the specific worths of both aluminum and water are slightly less for the larger sample (B) than for the smaller sample (A).

In the case of sample B, the various aluminum weights were obtained by using rods of different weights as well as by using sleeves. Thus, about the same weight variations resulted for both rods and sleeves, but the spatial distributions within the sample were different. In the center location, a plot of the two sets of data exhibited only random scatter about a common line. Hence, a single line was fitted to these data. In the corner location, a plot of the two sets of data indicated two obviously different functional relationships. Hence, these data were fitted separately for rods and sleeves. No significant difference in water worth was noted whether rods or sleeves were used. The aluminum worth difference, however, is inconclusive because of the large uncertainty in the value for the rods.

In general, it may be concluded that the reactivity worths of aluminum and water in the center location are not significantly affected by sample geometry up to the size of sample B. In the corner location, a signficant difference is noted for both aluminum and water.

5. REFERENCES

1. R. L. Tromp, "Swelling of Irradiated Beryllium", Nuclear Technology Branches Quarterly Report, April 1-June 30, 1965, IDO-17140 (unpublished).

2. G. I. Novikova et al, "Radioactive Decay of Ac^{227} and Excited Levels of Fr^{223} and Th^{227}", Sov. Phys. JETP, 10, No. 4 (April 1960) pp 663-669.

3. K. S. Singwi, "Coherent Scattering of Slow Neutrons by a Liquid", Phys. Rev., 136 (November 1964) pp A969-980.

4. G. H. Vineyard, "Scattering of Slow Neutrons by a Liquid", Phys. Rev., 110 (June 1958) pp A999-1010.

5. P. D. Randolph, "Slow Neutron Inelastic Scattering from Liquid Sodium", Phys. Rev., 134 (June 1964) pp A1238-1248.

6. P. A. Egelstaff and P. Schofield, "On the Evaluation of the Thermal Neutron Scattering Law", Nucl. Sci. Eng., 12 (February 1962) pp 260-270.

7. R. Kaplow, S. L. Strong, and B. L. Averback, "Radial Density Functions for Liquid Mercury and Lead", Phys. Rev., 138 (May 1965) pp A1336-1345.

8. S. J. Cocking and P. A. Egelstaff, "Frequency-Wave Number Relationship for Cooperative Modes of Motion in Liquid Lead and Tin", Phys. Letters, 16, No. 2 (May 1965) pp 130-132.

III. MATHEMATICAL ANALYSIS AND MACHINE COMPUTATIONS

1. PLOT ALL (PLØTAL) (PPCo 40.0471)

(G. A. Cazier, L. M. Wagner)

A multiple purpose plot program has been developed for the IBM 7040 Calcomp plotter system. This program was designed specifically to plot gamma-ray spectra with three different options available:

(1) Plot each spectra on separate plots, all with the same symbol.

(2) Plot a set of spectra on one graph with the first spectrum plotted with the symbol "□" and all others with lines.

(3) Plot a set of spectra (less than or equal to 5) on one graph, with a different symbol for each spectrum. The order of the symbols is "X", "□", "*", "line", and "◇".

All the plots are semilog where the "y" values are $\log_{10}$ of the counts per channel and the "x" values are the channel numbers. Up to 5000 channels may be plotted in each spectra. The size of the plot may be specified by the user.

2. TRANSFER SUMMARY REPORT (PPCo 40.0390)

(A. T. Reddish)

An IBM 7040 CØBØL Program has been completed which processes the information on receipts and shipments of radioactive material from the five stations at the NRTS. Reports are prepared on the transfer of all radioactive material to and from the site and organized according to station and type of material.

3. WAREHOUSE CATALOG PROGRAM (PPCo 40.0318)

(A. T. Reddish)

An IBM 7040 CØBØL Program has been written which prepares stock inventory catalogs for the CFA, CPP, and TRA areas.

The CFA catalog is divided into fourteen different classes. All items within each class are sorted in alphabetical order. An index was prepared for all unique items and was organized also in alphabetical order so that stock items could be easily located.

The CPP and TRA area catalogs were prepared with major component stock items listed first and all spare parts for this particular stock item listed after. The major stock items were sorted according to equipment number while the spare parts were sorted in alphabetical order. Indexes were also prepared for these catalogs.

Additional programs were written which enable changes (additions and deletions) to be made to each catalog.

4. LOFT BLØWDØWN PROGRAM (PPCo 40.0527)

(G. A. Jayne)

An IBM 7040 FØRTRAN program, BLØWDØWN, is used to study the behavior of pressurized fluid in a cylindrical vessel immediately subsequent to a rupture in the end of the vessel. Mass velocity, pressure, and enthalpy are computed for a specified number of mesh points along the length of the vessel and for a given number of time steps. Derivatives are computed by using difference equations on the previous time-step values of those three quantities.

The present version assumes a subcooled liquid only, but the capability of considering both liquid and gas is now being developed.

5. NRTS LIBRARY CATALOG (PPCo 40.0427)

(G. A. Jayne)

MECHANICAL MAID MARIAN, and IBM 7040 CØBØL program, is being written to prepare a master magnetic tape catalog of all NRTS library books. Updating and editing of this tape will be possible. Many alphabetized listings will be obtainable, including Author Catalog, Title Catalog, Subject Catalog, Call Number Catalog, Catalog of Symposia, and Catalog of Reference Books.

6. NRTS LIBRARY MONTHLY BOOK LIST (PPCo 40.0341)

(G. A. Jayne)

An IBM 7040 CØBØL program has been written which prepares current listings of newly acquired books at the NRTS Library.

7. GAUSSIAN INTEGRATION WITH WEIGHT FUNCTIONS OF SIN OR COS

(David A. Yokers)

Numerical integration uses a summation process to approximate an integral. Gaussian integration is a particular method of numerical integration, usually represented as

$$\int_a^b W(x)\, f(x)\, dx \approx \sum_{i=1}^{n} H_i\, f(x_i)$$

for $W(x) \geq 0$ and $a < x < b$. Tables of Gaussian integration weights H_k and abscissae x_k for various W(x), and intervals $a < x < b$ exist in the literature[a]. The advantages of Gaussian integration include: the formula is exact for f(x), a polynomial of degrees 2n-1 or less; the weight function does not have to be evaluated; a "near-optimum" utilization of a fixed number of evaluations of the integrand; and problems with integrably singular weight functions and/or infinite intervals of integration can be treated. A disadvantage of the Gaussian-type integration is that the evaluations of the integrand cannot be used when going from an n- to an m-point integration formula. Also, the difficulties in generating high-order, high-precision weights and abscissae for a given weight function and interval prevent using Gaussian integration unless the required tables are available. Several programs were written for generating the weights and abscissae for the weight functions sin x in the interval $0 < x < \pi$ and cos x in the interval $0 < x < \pi/2$.

7.1 Weight Generator for Gaussian Integration (PPCo 40.0577)

This program computes the weights, H_i, which occur in the Gaussian integration formula

$$\int_a^b W(x)\, f(x)\, dx = \sum_{i=1}^{n} H_i\, f(x_i)$$

where the x_i are the roots of the nth degree polynomial which is orthogonal with respect to W(x) over the interval (a,b,).

7.2 Generator of Orthogonal Polynomials -- Sin(x) (PPCo 40.0578)

This program generates the coefficients of polynomials $P_n(x)$ which are orthogonal over the interval $(0,\pi)$ with respect to the weighting function sin x.

7.3 Generation of Orthogonal Polynomials -- Cos(x) (PPCo 40.0579)

This program generates the coefficients of polynomials $P_n(x)$ which are orthogonal over the interval $(0,\pi/2)$ with respect to the weighting function cos x.

Following is a tabulation of these abscissae and the corresponding weights, from n = 2 to n = 7, for the weight function cos x, $0 \leq x \leq \pi/2$:

n = 2

x_i	H_i
$2.6587\ 38806 * 10^{-1}$	0.60362 55331
1.0351 52609	0.39637 44668

[a] References -- Gaussian Quadurative Formulae for $\int_0^1 -\ell n(x)\, f(x)\, dy$, Donald G. Anderson, Mathematics of Computation, July 1965

n = 3

$1.5009\ 31400*10^{-1}$	0.36401 26926
$6.6618\ 24711*10^{-1}$	0.47684 23234
1.2472 68475	0.15914 49840

n = 4

$9.5669\ 38920*10^{-2}$	0.23783 07142
$4.5240\ 90233*10^{-1}$	0.40265 69552
$9.3185\ 05767*10^{-1}$	0.28681 73795
1.3564 43960	$0.72694\ 95108*10^{-1}$

n = 5

x_i	H_i
$6.6100\ 65840*10^{-2}$	0.16623 94991
$3.2359\ 72325*10^{-1}$	0.31729 62312
$7.0306\ 74906*10^{-1}$	0.31034 19072
1.1020 26520	0.16893 42366
1.4190 09106	$0.37188\ 12598*10^{-1}$

n = 6

$4.8341\ 24388*10^{-2}$	0.12234 10835
$2.4159\ 13699*10^{-1}$	0.24090 09195
$5.4244\ 36535*10^{-1}$	0.28666 29006
$8.8891\ 10499*10^{-1}$	0.21870 83586
1.2145 81997	0.10249 90402
1.4579 24839	$0.20799\ 69756*10^{-1}$

n = 7

$3.5721\ 59349*10^{-2}$	$0.90843\ 09746*10^{-1}$
$1.8163\ 30051*10^{-1}$	0.19372 68238
$4.1922\ 96753*10^{-1}$	0.24846 18641
$7.1190\ 22336*10^{-1}$	0.23164 81681
1.0159 81494	0.15517 89267
1.2862 85275	$0.67106\ 27566*10^{-1}$
1.4817 14255	$0.13034\ 84420*10^{-1}$

Following is a tabulation of these abscissae and the corresponding weights, from n = 2 to n = 9 for the weight function $\sin x, 0 \le x \le \pi$:

n =2

x_i	H_i
8.8712 89367*10^{-1}	1.0000 00000
2.2544 63717	1.0000 00000

n = 3

5.5819 50868*10^{-1}	0.45584 04080
1.5707 96327	0.10883 19184*10^{1}
2.5833 97567	0.45584 04080

n = 4

x_i	H_i
3.8011 97629*10^{-1}	0.22407 06181
1.1315 08860	0.77592 93819
2.0100 83794	0.77592 93819
2.7614 72891	0.22407 06181

n = 5

2.7435 60467*10^{-1}	0.12011 19982
8.4480 95888*10^{-1}	0.50378 25124
1.5707 96327	0.75221 09788
2.2967 83065	0.50378 25124
2.8672 36607	0.12011 19982

n = 6

2.0688 50257*10^{-1}	0.69387 74905*10^{-1}
6.5100 56630*10^{-1}	0.32479 85521
1.2469 44213	0.60581 36988
1.8946 48440	0.60581 36988
2.4905 86991	0.32479 85521
2.9347 07628	0.69387 74905*10^{-1}

n = 7

1.6137 89680*10^{-1}	0.42625 51413*10^{-1}
5.1525 53363*10^{-1}	0.21352 96423
1.0072 93496	0.45607 41377
1.5707 96327	0.57554 14116
2.1342 99158	0.45607 41377
2.6263 37317	0.21352 96423
2.9802 13686	0.42625 51413*10^{-1}

n = 8

x_i	H_i
1.2930 88322*10^{-1}	0.27536 88562*10^{-1}
4.1707 87677*10^{-1}	0.14420 85135
8.2733 75524*10^{-1}	0.33626 63425
1.3143 04386	0.49198 82583
1.8272 88268	0.49198 82583
2.3142 55101	0.33626 63425
2.7245 13886	0.14420 85135
3.0122 83821	0.27536 88562*10^{-1}

n = 9

1.0793 07348*10^{-1}	0.19227 33111*10^{-1}
3.4925 10480*10^{-1}	0.10250 97668
6.9651 41443*10^{-1}	0.24969 20988
1.1157 18794	0.39805 68275
1.5707 96327	0.46102 79518
2.0258 73860	0.39805 68275
2.4450 78509	0.24969 20988
2.7923 41606	0.10250 97668
3.0336 61919	0.19227 33111*10^{-1}

8. SUMIT -- NUMERICAL EVALUATION OF AN INTEGRAL WITH A DAMPED OSCILLATING INTEGRAND SUBROUTINE (PPCo 40.0582)

(David A. Yokers)

This subroutine computes

$$\int_0^\infty \exp\left(-a_1x - a_2x^2\right) \sin a_3x \, dx$$

or

$$\int_0^\infty \exp\left(-a_1x - a_2x^2\right) \cos a_3x \, dx$$

where

$a_1 \geq 0$

$a_2 \geq 0$

$a_3 > 0$.

A transformation is made such that the integral is represented by a sum of an alternating series whose terms are integrals with limits such that the trigonmetric function is plus or minus in the interval. The integrals of each term (with suitable transformations) are evaluated using the eight-point Gaussian integration formula. (See tables included elsewhere in this report.) Convergence of the series is accelerated by using the ϵ-algorithm.

9. CONVERSION OF PROGRAMS TO THE IBM 7040

(John R. Bower)

The following computer programs were converted for use on the IBM 7040 computer:

EIG4, Complex Matrix Eigenvalue Subroutine (PPCo 40.0529). (Conversion of SHARE No. 7090-3099 NYU)

WRIMC, Complex Matrix Read-Write Subroutine (PPCo 40.0542). (Modification of WRIM, PPCo 40.0333)

EIG4P, Complex Matrix Eigenvalue Program. (PPCo 40.0543). This program is used when a requester has a given matrix and wants the eigenvalues. [EIG4 (PPCo 40.0529) is a subroutine that computes the eigenvalue for use in another computer program.]

Gamma Function of a Real Number (PPCo 40.0548). (Conversion of SHARE 7090-3155 NBS GAM.)

Inverse Error Function Subroutine (PPCo 40.0549). (Conversion and Modification of SHARE 7090-3154 NBS ERFI.)

Given y,

$$y = \frac{2}{\sqrt{\pi}} \int_0^x e^{-t^2} dt, \text{ this subroutine finds } x.$$

Eigenvectors of a Complex Matrix Subroutine (PPCo 40.0550)

Eigenvalues and Eigenvectors of a Real Symmetric Matrix Subroutine (PPCo 40.0566). (Conversion of Argonne National Laboratory program AN F202).

Eigenvalues and Eigenvectors of a Complex Matrix (PPCo 40.0569). (The user supplies the complex matrix, and the program prints the eigenvalues and eigenvectors. The subroutines, PPCo 40.0529 and 40.0550, should be used if the values are to be used in another computer program.)

Eigenvalues and Eigenvectors of a Real Symmetric Matrix (PPCo 40.0571). Use this program when one has a given matrix and wants the eigenvalues and vectors as the end result. Use the subroutine 40.0566 when one wants the eigenvalues and vectors for use in another computer program.

10. CROSS-SECTION PROGRAMS FOR BOMB TEST DATA

(Neldon Marshall)

Version 1 of the cross-section code is debugged and working. Several auxiliary codes to edit input tapes, average output data, and produce cross sections have also been written and debugged.

Work has been started in the study of the unfolding or unconvoluting problem. Several approaches are under study at the present time.

PHILLIPS
PETROLEUM
COMPANY

ATOMIC ENERGY DIVISION